A general characterisation of space-time prisms with spatial anchor uncertainty

Peer-reviewed author version

JANSEN, Arthur & KUIJPERS, Bart (2024) A general characterisation of space-time prisms with spatial anchor uncertainty. In: International journal of geographical information science, 38 (6) , p. 1035 -1064.

DOI: 10.1080/13658816.2024.2332631
Handle: http://hdl.handle.net/1942/45686

ARTICLE TEMPLATE

A general characterisation of space-time prisms with spatial anchor uncertainty

Arthur Jansen[a] and Bart Kuijpers[a]

[a]Databases and Theoretical Computer Science Group and Data Science Institute (DSI), Hasselt University and transnational University Limburg, 3500 Hasselt, Belgium

ARTICLE HISTORY
Compiled March 13, 2024

ABSTRACT
We investigate the geometry of space-time prisms and their associated potential path areas (for movement that takes place in the plane) in the setting where the prism anchors have a spatial uncertainty area attached to them. Our main result is a characterisation of such space-time prisms and their potential path areas in terms of a generalised distance function between closed subsets of the ambient space. Since the case where this spatial anchor uncertainty takes the form of a closed disk has already been addressed by Kuijpers and Othman (2017), we focus on the more realistic case where the uncertainty areas are ellipses and we apply our general characterisation to this example to obtain explicit descriptions of the uncertain prisms and their potential path areas.

KEYWORDS
Moving objects; Space-time prisms; Potential path area; Anchor uncertainty; Generalized ellipses

1. Introduction

The proliferation of portable location aware devices (such as, mobile phones, GPS and Bluetooth), during the past decades, has resulted in the collection and availability of huge data sets of time-stamped locations of moving objects (Giannotti and Pedreschi 2008). Such data represent (partial) *trajectories* of objects that move, for example, in a two-dimensional plane or along some transportation network. Their collected movement data is essentially discrete in nature and can be seen as a sequence $\langle(x_0, y_0, t_0), (x_1, y_1, t_1), ..., (x_n, y_n, t_n)\rangle$ of measured space-time locations, with increasing time values $t_0 < t_1 < \cdots < t_n$. Such a sequence is called a *trajectory sample* and between sampled space-time points, the trajectories are unspecified and unknown. Already in the early 2000s techniques have been proposed, both in the GIS and spatio-temporal database communities, to reconstruct trajectories from a given measured samples. These techniques include linear interpolation and uncertainty cylinders and they produce realistic results for frequently sampled moving objects (Güting and Schneider 2005, Trajcevski *et al.* 2004, Wolfson 2002).

The problem of the *uncertainty* of the space-time locations of moving objects in between measured space-time points has received much research attention in the past

CONTACT Arthur Jansen. Email: arthur.jansen@uhasselt.be

two decades and the *space-time prism* model, a technique coming from "time geography", has played a prominent role in this development. Space-time prisms were first proposed by Hägerstrand (1970) to study and analyse the potentiality of human activity. They entered the GIS community in the 1990s in the work of Miller (1991) and the spatio-temporal database research in the early 2000s in the work of Egenhofer (2003). The space-time prism model relies on the knowledge of speed bounds for the moving objects between trajectory sample points and based on these speed bounds a region of space-time can be delimited which a moving object may have visited. Geometrically seen, space-time prisms are the intersection of two space-time cones (one pointing to the future and one to the past). In this context, trajectory sample points are referred to as the *anchor points* of the prism. The spatial projection of a space-time prism contains all spatial locations that a moving object may have visited in the available time interval, given the anchor points and the speed bounds. Indeed, all physically possible spatio-temporal paths are located in this area and is referred to as the "potential path area" (PPA) or the "activity space" (AS) (see, for example, (Patterson and Farber 2015)).

We remark that, in our setting, besides the uncertainty of the space-time locations between sample points, there are several other sources of uncertainty. These include spatial and temporal measurement errors, outliers in the observations and missing data. Several attempts were already made to take these additional sources of uncertainty into account. For example, in Kuijpers *et al.* (2010), Othman (2009), both the spatial and temporal uncertainty on the measurement of anchor points are studied in the context of movement on a transportation network. In the presence of high precision clocks (for example, carried by satellites), temporal uncertainty is less important and in Kuijpers and Othman (2017) the spatial uncertainty on the anchor points was studied by modelling it in terms of "error disks" that are centered in the measured location.

The main contribution of the present paper is that we generalise the result of Kuijpers and Othman (2017) from error disks to "arbitrary error regions" in the two-dimensional plane. We give a general characterisation of both the space-time prism and the potential path area in the case where anchor points are located in some uncertainty region (that is the result, for example, of some measurement error). Our characterisation is based on a distance function between two subsets of the plane which generalises the classical Euclidean distance between points in the plane. Using this distance function, we see that space-time prisms with uncertain anchor regions are natural generalisations of classical prisms. The same is true for their potential path areas, which in the classical setting are ellipses and which in the presence of anchor uncertainty can be regarded as "generalised ellipses" (Ochkov *et al.* 2019). In particular, they are ellipses which have the two uncertainty regions as foci. We remark that the above mentioned general results can be applied in many settings. These include movement on transportation networks, but we mention that in that context prisms with uncertain anchors were already studied by Kuijpers and Othman (2009) and also by Othman (2009).

Next, this paper is devoted to applying this general result to the case where anchor uncertainty regions are *elliptical*. In this way, we generalise the results of Kuijpers and Othman (2017), since disks are special cases of ellipses. We also obtain a more realistic setting since the error regions derived from Global Navigation Satellite System (GNSS) positioning solutions rather have elliptical shapes than circular ones (Kaplan and Hegarty 2017). Another example of elliptical error regions is provided by the Argos satellite telemetry system (Argos 2018), which is popular in animal ecology, where it is used for tracking movement of for example marine animals. With each satellite fix, the Argos system provides locations accompanied with an estimated error ellipses. McClintock *et al.* (2015) work with such Argos data in studying the bearded seal and the Hawaiian monk seal and they claim that "the (Argos) location error ellipse has yet to be incorporated into analyses of animal movement". This gives an example of an area where the results of the present paper could be applied and towards the end of this paper, we provide some application scenarios.

Apart from this application-related motivation, we also study error ellipses with the complexity of the associated uncertain prisms and uncertain potential path areas in mind. As our study shows, the geometry of these geometric figures exceeds the complexity of the case of circular error regions extensively. Whereas uncertain prisms with circular anchor uncertainty are truncated classical prisms (and can be therefore described by polynomial inequalities of degree two), as shown by Kuijpers and Othman (2017), uncertain prisms with elliptical anchor uncertainty need polynomials of degree eight to describe them and their geometry is quite complicated. We give an explicit description of these prisms and show that they are, at any moment in the time interval of the ellipse, described by curves that are known as *toroids*. A description of the associated uncertain potential path areas is even more intricate and we give a less complicated way to approximate them by so-called 4-ellipses in an appendix.

A returning issue in the study of uncertain prisms and uncertain potential path areas in the context of anchor uncertainty that is elliptical is that of quantifier elimination: often it is easy to describe such sets by formulas that contain quantifiers. However, such formulas are not very useful, for example, for testing membership of he geometric set in question or for their drawing. This issue has been extensively studied in the context of "constraint databases" (Paredaens *et al.* 2000), in which geometric figures are required to be described by Boolean combinations of polynomial inequalities (without quantifiers). In real algebraic geometry, algorithms are studied that perform quantifier elimination, but due to their high computational complexity, these algorithms are of limited practical use (Bochnak *et al.* 1998). We pursue to have quantifier-free descriptions of uncertain prisms and uncertain potential path areas and much effort is devoted, in this paper, to obtain them. For the uncertain potential path areas this turns out to be complicated, in general. In particular case where the uncertainty regions are disks, we obtain an explicit description of the uncertain potential path area, which is a truncated ellipse (a result that was missing in Kuijpers and Othman (2017), where uncertain prisms were characterised as truncated classical prisms).

Organisation of the paper. In Section 3, we review classical space-time prisms and and their potential path areas and give the definitions of these concepts in the case of spatial anchor uncertainty (adapted from Kuijpers and Othman (2017)). In Section 4, we present a general characterisation of uncertain prisms and their uncertain potential path areas in terms of a distance function between subsets of the plane. In Section 5, we apply the general results to space-time prisms with elliptical anchor uncertainty regions and in Section 6, we discuss the corresponding potential path areas. Section 7 presents some application scenarios. The paper concludes with a discussion and open problems in Section 8.

2. Related work

Space-time prisms first appeared in the area of *time geography* in the earlier work of Hägerstrand (1970). Soon thereafter, their geometric properties and applications to the study of human activity planning and analysis were developed (Burns 1979, Lenntorp 1976). In the early 1990s, prims were introduced to the wider GIS community (see, for example, the work of Miller (1991)) and in the early 2000s, they found their way to spatial and spatio-temporal database research, where they were initially called "beads" in Egenhofer (2003). Later on, the space-time prism model has found its way into *Moving Object Databases* (MODs) (Wolfson 2002, Trajcevski *et al.* 2004, Güting and Schneider 2005) and also into the theory of such database systems (Othman 2009, Kuijpers and Othman 2010).

The introduction of space-time prisms in these new fields also brought with it a shift in their details, purpose and use. Initially, in the context of time geography, prisms were based on human-recorded activity (describing roughly the locations and times of activities in a log book, for example) and they had their use in planning and determining the feasibility of activities and the description of the constraints of humans, as is clear from the books of Burns (1979) and Lenntorp (1976). However, in the context of GIS and spatio-temporal databases, their purpose shifted towards modeling the uncertainty of the space-time locations in between measured anchors (Egenhofer 2003) in order to reconstruct the moving object's trajectories as an improvement on simple linear interpolation (Wolfson 2002, Trajcevski *et al.* 2004). With the proliferation of location-aware devices, such as GPS, the recording of the measured anchors also moved from hand-written to fairly precise. In the context of satellite-based measurements, location imprecision of some shape may still occur, but temporal measurements can be considered extremely accurate.

Whereas the original space-time prisms were concerned with free movement in a two-dimensional environment, they were later on also adapted to more constrained movement on transportation network (Miller 1991, Kwan and Hong 1998, Wu and Miller 2002, Kuijpers and Othman 2009) and other constrained spaces (Delafontaine *et al.* 2011).

With the development of computational and analytic tools for prisms (Kwan and Hong 1998, Miller 1991, 2005a,b, Yu and Shaw 2008), they have found applications in transportation planning (Timmermans *et al.* 2002), crime analysis (Kwan 1999, Ratcliffe 2006) and risk assessment (for example, in relation to epidemics and environmental problems) (Jacquez 2000, Jacquez *et al.* 2005, Löytönen 1998).

For what concerns the uncertainty on the measurement of anchor points, early work considered a Gaussian distribution for movement in the two-dimensional plane and this probabilistic approach was also extended to deal with anchor uncertainty of prisms on road networks by Pfoser *et al.* (2005). We already mentioned Kuijpers *et al.* (2010) and Othman (2009), in which both the spatial and temporal uncertainty of anchor points are considered in a probabilistic context for movement on a transportation network and the propagation of these probabilities in the space-time prism is studied. For movement in constrained spaces with obstacles, the combinations of spatial and temporal uncertainty are considered by Delafontaine *et al.* (2011).

For self-reported activity, temporal uncertainty is more important (Chen *et al.* 2013, Liao *et al.* 2014). In this paper, we ignore temporal uncertainty on anchor points., as was done by Kuijpers and Othman (2017), from which we adopted the definition of an uncertain prism and its potential path area.

3. Space-time prisms with spatial anchor uncertainty

In this section, we review the definitions of classical space-time prisms and their potential path areas. Next, we generalize the definitions by Kuijpers and Othman (2017) for the case where spatial uncertainty areas are attached to the anchors of the prism.

We start by giving some notational conventions that are used throughout this paper. We denote the set of the real numbers by $\mathbb{R}$. We consider movement in the two-dimensional plane and the corresponding spatio-temporal space is then modelled as $\mathbb{R}^2 \times \mathbb{R}$, in which $\mathbb{R}^2$ is the *spatial* component (where the movement takes place) and in which the last component $\mathbb{R}$ is used to model the *temporal* dimension. We use $p, q, ...$ (with or without indices) to refer to spatial points in $\mathbb{R}^2$ and t (with or without indices) to refer to the time moments. With this notation, we write (p, t) for a space-time point in $\mathbb{R}^2 \times \mathbb{R}$. Whenever we need coordinates (x, y) for a spatial point p, we denote the spatio-temporal point (p, t) by (x, y, t). Finally, we denote the standard Euclidean distance function on $\mathbb{R}^2$ by d.

3.1. *Classical space-time prisms and their potential path areas*

In this section, we give the definition of classical space-time prisms and their potential path areas for movement in $\mathbb{R}^2$.

3.1.1. Classical space-time prisms

Space-time prisms are usually applied in a context where trajectories of moving objects are recorded as a discrete sample $\langle (p_0, t_0), (p_1, t_1), ..., (p_n, t_n) \rangle$ of space-time points in $\mathbb{R}^2 \times \mathbb{R}$, which can be considered as an ordered sequence, following the order on the time coordinate, $t_0 < t_1 < \cdots < t_N$. We call such a sequence of spatio-temporal points a *trajectory sample* and the space-time points in it are referred to as *sample points*. In between two sample points (p_i, t_i) and (p_{i+1}, t_{i+1}), the location of the moving object is not recorded and thus unknown. However, when a maximal speed $v_{\max} > 0$ is known for the moving object, the possible space-time locations that a moving object may potentially have visited between these sample points can be described by the well-known space-time prism model (Burns 1979, Lenntorp 1976), of which we give the definition next.

Definition 3.1. Let (p_i, t_i) and (p_{i+1}, t_{i+1}) be two spatio-temporal points in $\mathbb{R}^2 \times \mathbb{R}$, taken from a trajectory sample, for which $t_i < t_{i+1}$. Let $v_{\max} \in \mathbb{R}$, with $v_{\max} > 0$, be a speed bound of the moving object that produced these sample points. The *space-time prism* for the *anchor points* (p_i, t_i) and (p_{i+1}, t_{i+1}) and the *maximal speed* $v_{\max}$, denoted by $\mathcal{P}(p_i, t_i, p_{i+1}, t_{i+1}, v_{\max})$, is defined to be the intersection of two cones in $\mathbb{R}^2 \times \mathbb{R}$, being

(1) *the bottom (or future) cone* $\mathsf{C}^-(p_i, , t_i, v_{\max}) := \{(p, t) \in \mathbb{R}^2 \times \mathbb{R} \mid d(p, p_i) \leq v_{\max} \cdot (t - t_i) \wedge t_i \leq t\}$ and
(2) the *top (or past) cone* $\mathsf{C}^+(p_{i+1}, t_{i+1}, v_{\max}) := \{(p, t) \in \mathbb{R}^2 \times \mathbb{R} \mid d(p, p_{i+1}) \leq v_{\max} \cdot (t_{i+1} - t) \wedge t \leq t_{i+1}\}$.

□

Therefore, the prism $\mathcal{P}(p_i, t_i, p_{i+1}, t_{i+1}, v_{\max})$ is the set of all space-time points (p, t)

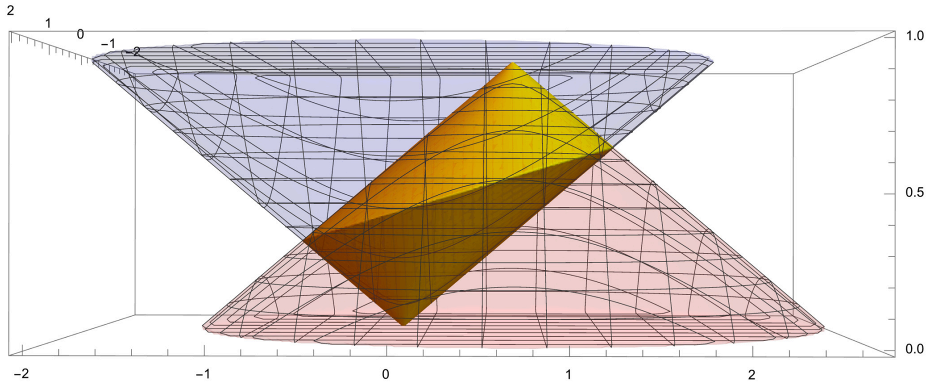

Figure 1. An illustration of a classical space-time prism $\mathcal{P}(x_i, y_i, t_i, x_{i+1}, y_{i+1}, t_{i+1}, v_{\max})$, in yellow, that is the intersection of the bottom cone $\mathsf{C}^-(x_i, y_i, , t_i, v_{\max})$, in blue, and the top cone $\mathsf{C}^+(x_{i+1}, y_{i+1}, t_{i+1}, v_{\max})$, in red.

that satisfy the formula

$$t_i \leq t \leq t_{i+1} \wedge d(p, p_i) \leq v_{\max} \cdot (t - t_i) \wedge d(p, p_{i+1}) \leq v_{\max} \cdot (t_{i+1} - t). \tag{1}$$

In this paper, we refer to such space-time prisms as *classical* space-time prisms. Figure 1 gives an illustration of a classical space-time prism.

3.1.2. Potential path areas of classical prisms

Next, we give the definition of the potential path area associated with the prism $\mathcal{P}(p_i, t_i, p_{i+1}, t_{i+1}, v_{\max})$. This is a subset of $\mathbb{R}^2$ that contains the spatial points that a moving objects may have visited when travelling from p_i to p_{i+1} in the time interval $[t_i, t_{i+1}]$, given the speed bound $v_{\max}$. It corresponds to the spatial projection of the prism, as the following definition shows. In this definition, we use the spatial projection $\pi_{\mathbb{R}^2} : \mathbb{R}^2 \times \mathbb{R} \to \mathbb{R}^2 : (x, y, t) \mapsto (x, y)$.

Definition 3.2. Given two anchor points (p_i, t_i) and (p_{i+1}, t_{i+1}) in $\mathbb{R}^2 \times \mathbb{R}$ and a speed bound $v_{\max} > 0$, the spatial projection $\pi_{\mathbb{R}^2}(\mathcal{P}(p_i, t_i, p_{i+1}, t_{i+1}, v_{\max}))$ of the prism $\mathcal{P}(p_i, t_i, p_{i+1}, t_{i+1}, v_{\max})$, is called its *potential path area* and it is denoted by $\mathsf{PPA}(p_i, t_i, p_{i+1}, t_{i+1}, v_{\max})$. □

From Definition 3.1, it follows that $\mathsf{PPA}(p_i, t_i, p_{i+1}, t_{i+1}, v_{\max})$ can be seen as the set of all $p \in \mathbb{R}^2$ that satisfy the quantified expression $\exists t \, (t_i \leq t \leq t_{i+1} \wedge d(p, p_i) \leq v_{\max} \cdot (t - t_i) \wedge d(p, p_{i+1}) \leq v_{\max} \cdot (t_{i+1} - t))$. However, for practical purposes (for example, to verify membership of a spatial point to the potential path area), such a quantified expression is not very useful. But it can be easily shown that the this expression is equivalent to the quantifier-free condition

$$d(p, p_i) + d(p, p_{i+1}) \leq v_{\max} \cdot (t_{i+1} - t_i). \tag{2}$$

This expression shows that the potential path area is a region enclosed by the ellipse with foci p_i and p_{i+1} and major axis $v_{\max} \cdot (t_{i+1} - t_i)$ (see (Burns 1979) and Chapter 4 in (Lenntorp 1976)).

3.2. *Space-time prisms with anchor uncertainty and their potential path areas*

In this section, we give the definition of space-time prisms with anchor uncertainty and their corresponding potential path areas for movement in the space $\mathbb{R}^2$. Instead of two anchor points (p_i, t_i) and (p_{i+1}, t_{i+1}) in $\mathbb{R}^2 \times \mathbb{R}$ (with $t_i < t_{i+1}$) and a speed bound $v_{\max} > 0$, we now have a region U_i at t_i, a region U_{i+1} at t_{i+1} and a a speed bound $v_{\max} > 0$. The regions U_i and U_{i+1} are subsets of $\mathbb{R}^2$ and the idea is that a moving object departs at t_i from some point in U_i and arrives at t_{i+1} at some point in U_{i+1}, travelling with maximal speed $v_{\max}$. We assume, in the remainder of this paper, that the uncertainty regions U_i and U_{i+1} are compact subsets of $\mathbb{R}^2$, meaning that they are bounded and topologically closed (the latter meaning, intuitively, that they contain their borders).

3.2.1. Space-time prisms with anchor uncertainty

The above idea is reflected in the following definition of a space-time prism with anchor uncertainty, which is a generalisation of (Kuijpers and Othman 2017).

Definition 3.3. The *space-time prism with anchor uncertainty* (or *uncertain prism*, for short) with the spatial uncertainty areas U_i at t_i and U_{i+1} at t_{i+1}, with $t_i < t_{i+1}$, and the maximal speed $v_{\max} > 0$ is denoted by $\mathcal{UP}(\mathsf{U}_i, t_i, \mathsf{U}_{i+1}, t_{i+1}, v_{\max})$ and is defined as

$$\bigcup_{p_i \in \mathsf{U}_i} \bigcup_{p_{i+1} \in \mathsf{U}_{i+1}} \mathcal{P}(p_i, t_i, p_{i+1}, t_{i+1}, v_{\max}).$$

□

When we write $\mathsf{UC}^-(\mathsf{U}_i, t_i, v_{\max})$ and $\mathsf{UC}^+(\mathsf{U}_{i+1}, t_{i+1}, v_{\max})$ for the sets $\bigcup_{p_i \in \mathsf{U}_i} \mathsf{C}^-(p_i, t_i, v_{\max})$ and $\bigcup_{p_{i+1} \in \mathsf{U}_{i+1}} \mathsf{C}^+(p_{i+1}, t_{i+1}, v_{\max})$, respecively, then it was established in (Kuijpers and Othman 2017), using elementary properties of sets, that $\mathcal{UP}(\mathsf{U}_i, t_i, \mathsf{U}_{i+1}, t_{i+1}, v_{\max}) = \mathsf{UC}^-(\mathsf{U}_i, t_i, v_{\max}) \cap \mathsf{UC}^+(\mathsf{U}_{i+1}, t_{i+1}, v_{\max})$. We call $\mathsf{UC}^-(\mathsf{U}_i, t_i, v_{\max})$ and $\mathsf{UC}^+(\mathsf{U}_{i+1}, t_{i+1}, v_{\max})$ the *bottom cone* and the *top cone* (of the space-time prism with anchor uncertainty), respectively. Technically speaking, these names are incorrect, as we will see later on, since these sets are not necessarily conic. However, this nomenclature is in line with that of classical prisms.

3.2.2. Potential path areas of space-time prisms with anchor uncertainty

The potential path area, associated with a uncertain space-time prism is defined, as before, to be its projection on the spatial plane. The potential path area consists of all points that a moving object could have visited (irrespective of time) when travelling from region U_i to a region U_{i+1} within the given speed bound. This is reflected in the following definition.

Definition 3.4. The *potential path area associated with the space-time prism with anchor uncertainty* (or *uncertain potential path area*, for short) of the uncertain prism $\mathcal{UP}(\mathsf{U}_i, t_i, \mathsf{U}_{i+1}, t_{i+1}, v_{\max})$ is defined as $\pi_{\mathbb{R}^2}(\mathcal{UP}(\mathsf{U}_i, t_i, \mathsf{U}_{i+1}, t_{i+1}, v_{\max}))$ and is denoted as $\mathsf{UPPA}(\mathsf{U}_i, t_i, \mathsf{U}_{i+1}, t_{i+1}, v_{\max})$. □

The following property shows that the uncertain potential path area can be seen as a union of classical potential path areas. Its proof simply follows from the fact that the spatial projection can be pushed through the unions of spatio-temporal sets.

Proposition 3.5. *We have*

$$\mathsf{UPPA}(\mathsf{U}_i, t_i, \mathsf{U}_{i+1}, t_{i+1}, v_{\max}) = \bigcup_{p_i \in \mathsf{U}_i} \bigcup_{p_{i+1} \in \mathsf{U}_{i+1}} \mathsf{PPA}(p_i, t_i, p_{i+1}, t_{i+1}, v_{\max}).$$

□

4. A general characterisation of uncertain prisms and their uncertain potential path areas

In this section, we give a general characterisation of uncertain prisms and of their uncertain potential path areas. This characterisation is based on a distance function between closed sets in the plane and it shows that, in terms of this distance function, uncertain prisms and their uncertain potential path areas can be seen as generalisations of classical space-time prisms and their potential path areas, which are defined in terms of the standard Euclidean distance.

First, we describe this (well-known) generalised concept of distance (between subsets of $\mathbb{R}^2$) (Kubrusly and Conci 2017). A natural extension of the standard distance function d of $\mathbb{R}^2$ to two subsets A and B of $\mathbb{R}^2$ is defined as

$$\bar{d}(A, B) = \inf\{d(a, b) \mid a \in A \text{ and } b \in B\}.$$

Since we work with compact (that is, closed and bounded) subsets of $\mathbb{R}^2$ in the following, we observe that the infimum in the definition is finite and attained and we thus have $\bar{d}(A, B) = \min\{d(a, b) \mid a \in A \text{ and } b \in B\}$. When A (or B) is a singleton $\{p\}$, we also write $\bar{d}(p, B)$. We remark that when both $A = \{p\}$ and $B = \{q\}$ are singletons, then $\bar{d}(p, q)$ coincides with their Euclidean distance $d(p, q)$, but in general $\bar{d}$ is not a metric (Kubrusly and Conci 2017).

4.1. *A characterization of prisms with anchor uncertainty in terms of the distance between subsets of* $\mathbb{R}^2$

Here, we give a description of space-time prisms with anchor uncertaint in terms of the generalised distance $\bar{d}$.

Theorem 4.1. *Let U_i and U_{i+1} be two (compact) uncertainty regions in $\mathbb{R}^2$, as described above. Let $t_i < t_{i+1}$ be two time moments and let $v_{\max} > 0$ be a speed bound. Then we have*

$$\begin{aligned}\mathcal{UP}(\mathsf{U}_i, t_i, \mathsf{U}_{i+1}, t_{i+1}, v_{\max}) = \{&(p, t) \in \mathbb{R}^2 \times \mathbb{R} \mid \\ &t_i \leq t \leq t_{i+1} \wedge \bar{d}(p, \mathsf{U}_i) \leq v_{\max} \cdot (t - t_i) \wedge \bar{d}(p, \mathsf{U}_{i+1}) \leq v_{\max} \cdot (t_{i+1} - t)\}.\end{aligned}$$

Before we proceed to proving this theorem, we remark that the formula that describes the space-time points that belong to $\mathcal{UP}(\mathsf{U}_i, t_i, \mathsf{U}_{i+1}, t_{i+1}, v_{\max})$ is a generalisation (now using $\bar{d}$ instead of d) of expression (1), that describes classical prisms.

Proof. We abbreviate the uncertain prism in the statement of the theorem by $\mathcal{UP}$ and the spatio-temporal set $\{(p,t) \in \mathbb{R}^2 \times \mathbb{R} \mid t_i \leq t \leq t_{i+1} \wedge \bar{d}(p, \mathsf{U}_i) \leq v_{\max} \cdot (t - t_i) \wedge \bar{d}(p, \mathsf{U}_{i+1}) \leq v_{\max} \cdot (t_{i+1} - t)\}$ by ST. We need to show that $\mathcal{UP} = \mathsf{ST}$ and do this by proving the two set inclusions.

To prove the inclusion $\mathcal{UP} \subseteq \mathsf{ST}$, we take a point $(p,t) \in \mathcal{UP}$ and show that $(p,t) \in \mathsf{ST}$. If $(p,t) \in \mathcal{UP}$, this means that there exists a point $q_i \in \mathsf{U}_i$ and a point $q_{i+1} \in \mathsf{U}_{i+1}$ such that $d(p, q_i) \leq v_{\max} \cdot (t - t_i)$; $d(p, q_{i+1}) \leq v_{\max} \cdot (t_{i+1} - t)$ and $t_i \leq t \leq t_{i+1}$. Since $\bar{d}(p, \mathsf{U}_i)$ is a minimum (over U_i), we have $\bar{d}(p, \mathsf{U}_i) \leq d(p, q_i)$. Similarly, we have $\bar{d}(p, \mathsf{U}_{i+1}) \leq d(p, q_{i+1})$. Therefore, we have $\bar{d}(p, \mathsf{U}_i) \leq v_{\max} \cdot (t - t_i)$, $\bar{d}(p, \mathsf{U}_{i+1}) \leq v_{\max} \cdot (t_{i+1} - t)$ and $t_i \leq t \leq t_{i+1}$ and we have shown that $(p,t) \in \mathsf{ST}$.

To prove the inclusion $\mathsf{ST} \subseteq \mathcal{UP}$, we take a point $(p,t) \in \mathsf{ST}$ and show that $(p,t) \in \mathcal{UP}$. If $(p,t) \in \mathsf{ST}$, we have $\bar{d}(p, \mathsf{U}_i) \leq v_{\max} \cdot (t - t_i)$, $\bar{d}(p, \mathsf{U}_{i+1}) \leq v_{\max} \cdot (t_{i+1} - t)$ and $t_i \leq t \leq t_{i+1}$, by definition. Since U_i, U_{i+1} and $\{p\}$ are compact sets, the infima (in $\bar{d}$) are attained. This means that there exists a point $q_i \in \mathsf{U}_i$ and a point $q_{i+1} \in \mathsf{U}_{i+1}$ such that $\bar{d}(p, \mathsf{U}_i) = d(p, q_i)$ and $\bar{d}(p, \mathsf{U}_{i+1}) = d(p, q_{i+1})$. From the above inequalities, we thus obtain $d(p, q_i) \leq v_{\max} \cdot (t - t_i)$; $d(p, q_{i+1}) \leq v_{\max} \cdot (t_{i+1} - t)$ and $t_i \leq t \leq t_{i+1}$. This means that (p,t) belongs to the classical prism $\mathcal{P}(q_i, t_i, q_{i+1}, t_{i+1}, v_{\max})$, with $q_i \in \mathsf{U}_i$ and $q_{i+1} \in \mathsf{U}_{i+1}$, and thus $(p,t) \in \mathcal{UP}$. This concludes the proof of the second inclusion and the proof is finished. □

4.2. *A characterization of uncertain potential path areas in terms of the distance between subsets of* $\mathbb{R}^2$

In this section, we give a description of the uncertain potential path area in terms of the generalised distance $\bar{d}$.

Theorem 4.2. *Let* U_i *and* U_{i+1} *be two (compact) uncertainty regions in* $\mathbb{R}^2$*, as described above. Let* $t_i < t_{i+1}$ *be two time moments and let* $v_{\max} > 0$ *be a speed bound. Then we have*

$$\mathsf{UPPA}(\mathsf{U}_i, t_i, \mathsf{U}_{i+1}, t_{i+1}, v_{\max}) = \{p \in \mathbb{R}^2 \mid \bar{d}(p, \mathsf{U}_i) + \bar{d}(p, \mathsf{U}_{i+1}) \leq v_{\max} \cdot (t_{i+1} - t_i)\}.$$

Again, we remark that the formula that describes the spatial points that belong to $\mathsf{UPPA}(\mathsf{U}_i, t_i, \mathsf{U}_{i+1}, t_{i+1}, v_{\max})$ is a generalisation of expression (2) that describes the classical potential path area (now using $\bar{d}$ instead of d). The above theorem shows that the uncertain potential path area is an "generalised ellipse" (with respect to $\bar{d}$) with (generalised) foci U_i and U_{i+1} and major axis $v_{\max} \cdot (t_{i+1} - t_i)$ (Ochkov *et al.* 2019).

Proof. We abbreviate $\mathsf{UPPA}(\mathsf{U}_i, t_i, \mathsf{U}_{i+1}, t_{i+1}, v_{\max})$ by UPPA and the spatial set $\{p \in \mathbb{R}^2 \mid \bar{d}(p, \mathsf{U}_i) + \bar{d}(p, \mathsf{U}_{i+1}) \leq v_{\max} \cdot (t_{i+1} - t_i)\}$ by S. We need to show that $\mathsf{UPPA} = \mathsf{S}$ and do this by proving the two set inclusions.

To show that $\mathsf{UPPA} \subseteq \mathsf{S}$, we take a point $p \in \mathsf{UPPA}$ and show that $p \in \mathsf{S}$. If $p \in \mathsf{UPPA}$, this means that there exists a point $q_i \in \mathsf{U}_i$ and a point $q_{i+1} \in \mathsf{U}_{i+1}$ such that $d(p, q_i) + d(p, q_{i+1}) \leq v_{\max} \cdot (t_{i+1} - t_i)$. Since $\bar{d}(p, \mathsf{U}_i)$ is a minimum (over U_i), we have $\bar{d}(p, \mathsf{U}_i) \leq d(p, q_i)$. Similarly, we have $\bar{d}(p, \mathsf{U}_{i+1}) \leq d(p, q_{i+1})$. Therefore, we have $\bar{d}(p, \mathsf{U}_i) + \bar{d}(p, \mathsf{U}_{i+1}) \leq d(p, q_i) + d(p, q_{i+1}) \leq v_{\max} \cdot (t_{i+1} - t_i)$ and we have shown that $p \in \mathsf{S}$.

To show that $\mathsf{S} \subseteq \mathsf{UPPA}$, we take a point $p \in \mathsf{S}$ and show that $p \in \mathsf{UPPA}$. If $p \in \mathsf{S}$, we have $\bar{d}(p, \mathsf{U}_i) + \bar{d}(p, \mathsf{U}_{i+1}) \leq v_{\max} \cdot (t_{i+1} - t_i)$, by definition. Since U_i, U_{i+1} and $\{p\}$

are closed sets, the infima (in $\bar{d}$) are attained. This means we have a point $q_i \in \mathsf{U}_i$ and a point $q_{i+1} \in \mathsf{U}_{i+1}$ such that $\bar{d}(p, \mathsf{U}_i) = d(p, q_i)$ and $\bar{d}(p, \mathsf{U}_{i+1}) = d(p, q_{i+1})$. From $d(p, q_i) + d(p, q_{i+1}) = \bar{d}(p, \mathsf{U}_i) + \bar{d}(p, \mathsf{U}_{i+1})$ and $\bar{d}(p, \mathsf{U}_i) + \bar{d}(p, \mathsf{U}_{i+1}) \leq v_{\max} \cdot (t_{i+1} - t_i)$, it follows that $d(p, q_i) + d(p, q_{i+1}) \leq v_{\max} \cdot (t_{i+1} - t_i)$, which means that $p \in \mathsf{UPPA}$. This concludes the proof of the second inclusion and the proof is finished. □

5. Space-time prisms with elliptical anchor uncertainty regions

In the work of Kuijpers and Othman (2017), the case of circular anchor uncertainty regions is investigated (be it without a description of the potential path area). However, as we have argued in the Introduction, in the context where sample points of a trajectory are obtained by measuring devices, elliptical uncertainty regions are more realistic. This case is discussed in this section, where we apply the general results of Section 4, directly or indirectly, to the setting where U_i and U_{i+1} are regions delimited by ellipses. To make it clear that we work with ellipses, we change the notation to UE_i and UE_{i+1}, in this section. First, we describe how UE_i and UE_{i+1} are given in the context of what we refer to as *elliptical anchor uncertainty*. For UE_i, located in the plane given by $t = t_i$ (the case UE_{i+1} is similar), we assume that the elliptical region is given by the following parameters:

- the spatial center of the ellipse (x_i, y_i);
- its semi-major axis a_i;
- its semi-minor axis b_i; and
- the angle φ_i between the positive x-direction and the major axis of the ellipse.

The resulting elliptical uncertainty region in the plane $t = t_i$ is denoted by $\mathsf{UE}(x_i, y_i, a_i, b_i, \varphi_i)$, or UE_i, for short. Its bordering ellipse is denoted $\partial\mathsf{UE}(x_i, y_i, a_i, b_i, \varphi_i)$, or $\partial\mathsf{UE}_i$, for short. Figure 2 gives an illustration.

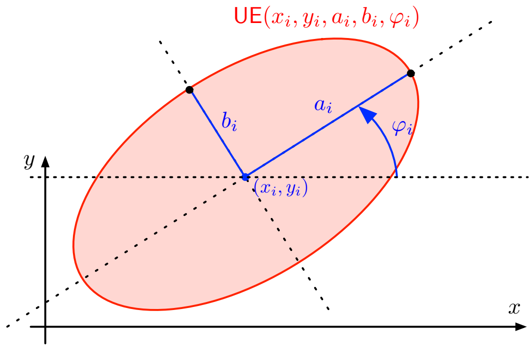

Figure 2. The elliptical uncertainty area $\mathsf{UE}(x_i, y_i, a_i, b_i, \varphi_i)$ is shown in red and is located in the spatial plane determined by $t = t_i$. Its red bordering curve is $\partial\mathsf{UE}(x_i, y_i, a_i, b_i, \varphi_i)$.

The ellipse $\partial\mathsf{UE}_i$, in the plane $t = t_i$, has the following (well-known) algebraic equation:

$$\frac{((x - x_i)\cos\varphi_i + (y - y_i)\sin\varphi_i)^2}{a_i^2} + \frac{(-(x - x_i)\sin\varphi_i + (y - y_i)\cos\varphi_i)^2}{b_i^2} = 1,$$

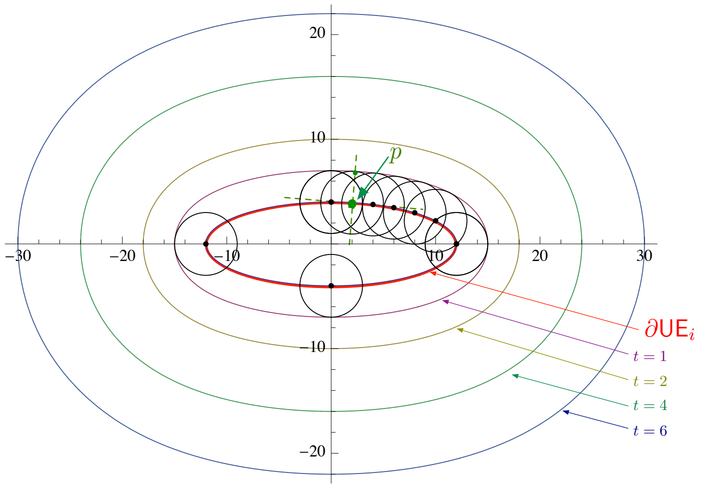

Figure 3. The elliptical curve $\partial\mathsf{UE}_i = \partial\mathsf{UE}(0, 0, a_i, b_i, 0°)$ is shown in red (for $a_i = 12$ and $b_i = 4$) and the construction of the point on a parallel curve (starting from the point $p \in \partial\mathsf{UE}_i$) is illustrated in green. The parallel curves for $v_{\max} = 3$ and $t = 1, 2, 4, 6$ are shown in various colours.

but also its parametric equation:

$$\begin{cases} x(\theta) &=& x_i + a_i \cos\theta \cos\varphi_i - b_i \sin\theta \sin\varphi_i \\ y(\theta) &=& y_i + a_i \cos\theta \sin\varphi_i + b_i \sin\theta \cos\varphi_i, \end{cases}$$

with parameter θ for $0 \le \theta < 2\pi$, is of use to us.

Now that we have fixed the notation for elliptical uncertainty regions, we explore the geometry of prisms with elliptical anchor uncertainty regions. Before giving their algebraic description, we explore the nature of the bottom cone of these uncertain prisms.

5.1. *Parametric and algebraic descriptions of the bottom cone of the prisms with elliptical anchor uncertainty*

To describe the bottom cone of the prisms with elliptical anchor uncertainty, we first study

$$\mathsf{UC}^-(\mathsf{UE}_i, t_i, v_{\max}) = \bigcup_{p_i \in \mathsf{UE}_i} \mathsf{C}^-(p_i, t_i, v_{\max}).$$

To reduce the length of the expressions, we look at $\mathsf{UE}_i = \mathsf{UE}(0, 0, a_i, b_i, 0°)$, located in the plane $t = 0$. This corresponds to an ellipse in standard position, centered at the origin of the plane, where the angle φ_i is taken to be $0°$. At moment t, with $t_i = 0 < t$, the spatial area that a moving object can be in is inscribed in the curve that is "parallel" to the (spatial projection of the) ellipse $\partial\mathsf{UE}_i$ with an "offset" of $v_{\max} \cdot (t - t_i)$, or $v_{\max} \cdot t$, for $t = 0$. To construct this curve, we can, at each point p of $\partial\mathsf{UE}_i$, construct a circle with radius $v_{\max} \cdot (t - t_i)$ and intersect this circle with the perpendicular line to the tangent to $\partial\mathsf{UE}_i$ in p. The outer intersection point then belongs to the parallel curve. This construction is illustrated in Figure 3.

For a curve with parametric description $x = f(\theta)$ and $y = g(\theta)$ (in the parameter θ), the equation of the parallel curve with outward offset d is given by $x_d(\theta) = f(\theta) +$

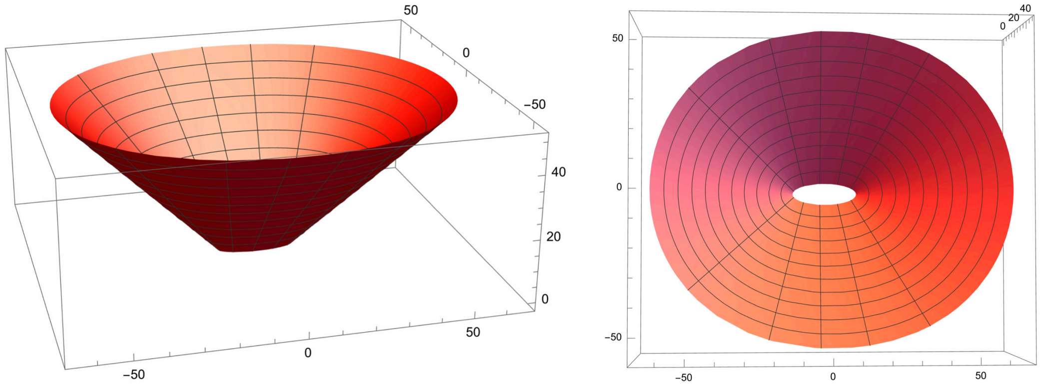

Figure 4. Two views of the mantel of the bottom cone for $0 \le t \le 50$ for $\mathsf{UE}_i = \mathsf{UE}(0, 0, 12, 4, 0°)$ and $v_{\max} = 3$. The second view is a top view and shows several toroids.

$\frac{d \cdot g'(\theta)}{\sqrt{f'(\theta)^2+g'(\theta)^2}}$ and $y_d(\theta) = g(\theta) - \frac{d \cdot f'(\theta)}{\sqrt{f'(\theta)^2+g'(\theta)^2}}$, in which the derivatives are taken with respect to θ (Gray 1997). When we use the parametric description $x = a_i \cos\theta$ and $y = b_i \sin\theta$ (with $0 \le \theta < 2\pi$) for the ellipse $\partial\mathsf{UE}_i$, we see that the curve parallel to $\partial\mathsf{UE}_i$ at time $t > t_i$ is given by the parametric equations

$$\begin{cases} x_t(\theta) &= (a_i + \frac{b_i \cdot v_{\max} \cdot t}{\sqrt{a_i^2 \sin^2\theta + b_i^2 \cos^2\theta}}) \cos\theta \\ y_t(\theta) &= (b_i + \frac{a_i \cdot v_{\max} \cdot t}{\sqrt{a_i^2 \sin^2\theta + b_i^2 \cos^2\theta}}) \sin\theta, \end{cases} \tag{3}$$

with $0 \le \theta < 2\pi$ (see also (Weisstein 2023)). These parallel curves are known as *toroids* (a name derived from the fact that they represent the visible outlines of the torus) and they were first studied by Cauchy in 1841 and were given their name by Catalan and Breton des Champs in 1844. Although they may look like ellipses (for instance, in Figure 3), they are actually algebraic curves of degree 8. Indeed, eliminating the parameter θ from Equations (3) produces the polynomial equation

$$\mathsf{Toroid}(x, y, a_i, b_i, v_{\max} \cdot (t - t_i)) = 0$$

of degree 8 (Weisstein 2023). The long expression for $\mathsf{Toroid}(x, y, a, b, d)$, given in Appendix A for the interested reader, is taken from (WoframAlpha 2023).

The collection of these toroids for all $t \ge t_i$ is then the mantel of the bottom cone. A side and top view of this mantel (produced using the parametric description) are given in Figure 4.

However, there is a problem with the equation $\mathsf{Toroid}(x, y, a, b, d) = 0$, namely that it produces two curves: one "outside" the ellipse (with positive offset d), together with one "inside" the ellipse (with negative offset $-d$). Indeed, in $\mathsf{Toroid}(x, y, a, b, d)$ the parameter d appears with even powers only, as a result of the elimination process. This is illustrated in the top part of Figure 5, where we see the two curves at offsets $d = 3$ and $d = -3$ (corresponding to $t = 1$) that satisfy the equation $\mathsf{Toroid}(x, y, a, b, d) = 0$ together with the ellipse they are parallel with (and the area enclosed by these two parallel curves). This figure might suggest that the ellipse itself separates the two curves, but this is not true for a larger offset, corresponding to a larger t, as is illustrated by the bottom half of Figure 5, which corresponds to $t = \frac{10}{3}$ or offsets $d = 10$ and $d = -10$.

To overcome this difficulty and to obtain a polynomial expression for the bottom

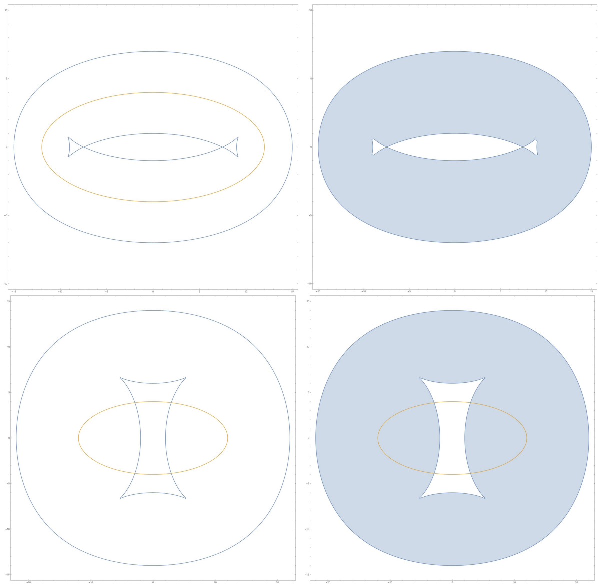

Figure 5. On the top left: the ellipse $\partial\mathsf{UE}_i(0, 0, 12, 4, 0°)$ (at $t_i = 0$) in yellow and the toroidal curves given by $\mathsf{Toroid}(x, y, 12, 4, 3) = 0$ (at $t = 1$ with $v_{\max} = 3$) in blue. On the top right: The set given by $\mathsf{Toroid}(x, y, 12, 4, 3) \leq 0$. On the bottom left the same curves and area are given for $t = \frac{10}{3}$.

cone of the prism with elliptical anchor uncertainty, we need to separate the inner from the outer offset curves. This is achieved by the following theorem that gives a description in terms of polynomial inequalities only.

Theorem 5.1. *Let UE_i be an elliptical uncertainty region located in the plane $t = t_i$ (with $t_i = 0$) that is enclosed by the ellipse $\partial\mathsf{UE}_i$ with equation $\frac{x^2}{a_i^2} + \frac{y^2}{b_i^2} = 1$, with $0 < b_i \leq a_i$. Let $v_{\max} > 0$ be a speed bound. The bottom cone of the uncertain prism with the standard ellipse UE_i as uncertainty region, at $t \geq t_i = 0$, then consists of the spatio-temporal points $(x, y, t) \in \mathbb{R}^2 \times \mathbb{R}$ that satisfy the following polynomial inequality formula:*

$$\begin{aligned}
&\varphi_{\mathsf{StUC}}(x, y, t, a_i, b_i, v_{\max}) := \\
&\qquad 0 \leq t \wedge \Big(\mathsf{Toroid}(x, y, a_i, b_i, v_{\max} \cdot t) \leq 0 \vee \frac{x^2}{a_i^2} + \frac{y^2}{b_i^2} \leq 1 \vee \\
&\qquad\quad \big(-a_i \leq x \leq a_i \wedge -v_{\max} \cdot (t - t_i) \leq y \leq v_{\max} \cdot t\big) \vee \\
&\qquad\qquad (x + a_i)^2 + y^2 \leq v_{\max}^2 \cdot t^2 \vee (x - a_i)^2 + y^2 \leq v_{\max}^2 \cdot t^2\Big).
\end{aligned}$$

□

The proof of the above theorem uses various geometrical argumentations and we refer the interested reader to Appendix B for the details.

5.2. *An algebraic description of the prisms with elliptical anchor uncertainty*

In this section, we give a description of the uncertain space-time prism

$$\mathcal{UP}(\mathsf{UE}_i, t_i, \mathsf{UE}_{i+1}, t_{i+1}, v_{\max}) = \mathsf{UC}^-(\mathsf{UE}_i, t_i, v_{\max}) \cap \mathsf{UC}^+(\mathsf{UE}_{i+1}, t_{i+1}, v_{\max}),$$

with elliptical anchor uncertainty regions $\mathsf{UE}_i = \mathsf{UE}(x_i, y_i, a_i, b_i, \varphi_i)$ at $t = t_i$ and $\mathsf{UE}_{i+1} = \mathsf{UE}(x_{i+1}, y_{i+1}, a_{i+1}, b_{i+1}, \varphi_{i+1})$ at $t = t_{i+1}$ (with $t_i < t_{i+1}$).

We use the result of Theorem 5.1 to obtain this description. Since the transformation

$$\begin{pmatrix} x \\ y \\ t \end{pmatrix} \mapsto \begin{pmatrix} \cos\varphi_i & -\sin\varphi_i & 0 \\ \sin\varphi_i & \cos\varphi_i & 0 \\ 0 & 0 & 1 \end{pmatrix} \begin{pmatrix} x \\ y \\ t \end{pmatrix} + \begin{pmatrix} x_i \\ y_i \\ t_i \end{pmatrix}$$

maps the standard ellipse $\mathsf{UE}(0, 0, a_i, b_i, 0°)$ at $t = 0$ to $\mathsf{UE}(x_i, y_i, a_i, b_i, \varphi_i)$ at $t = t_i$, we can use the inverse transformation to obtain a description of $\mathsf{UC}^-(\mathsf{UE}_i, t_i, v_{\max})$. Therefore, $\mathsf{UC}^-(\mathsf{UE}_i, t_i, v_{\max})$ consists of the points $(x, y, t) \in \mathbb{R}^2 \times \mathbb{R}$ that satisfy the formula

$$\begin{aligned} &\varphi_{\mathsf{UC}^-}(x, y, t, t_i, a_i, b_i, \varphi_i, v_{\max}) := \\ &\varphi_{\mathsf{StUC}}(\cos\varphi_i(x - x_i) + \sin\varphi_i(y - y_i), -\sin\varphi_i(x - x_i) + \cos\varphi_i(y - y_i), t - t_i, a_i, b_i, v_{\max}). \end{aligned}$$

Because of the presence of cosines and sines, this formula is no longer a description in terms of polynomial inequalities.

By a similar argumentation, now taking into account that time should be reversed, we obtain a description of the top cone:

$$\begin{aligned} \varphi_{\mathsf{UC}^+}(x, y, t, t_{i+1}, a_{i+1}, b_{i+1}, \varphi_{i+1}, v_{\max}) := \\ \varphi_{\mathsf{StUC}}(\cos\varphi_{i+1}(x - x_{i+1}) + \sin\varphi_{i+1}(y - y_{i+1}), \\ -\sin\varphi_{i+1}(x - x_{i+1}) + \cos\varphi_{i+1}(y - y_{i+1}), t_{i+1} - t, a_{i+1}, b_{i+1}, v_{\max}). \end{aligned}$$

We summarize these observations in the following theorem.

Theorem 5.2. *Let $\mathsf{UE}_i = \mathsf{UE}(x_i, y_i, a_i, b_i, \varphi_i)$ be an elliptical anchor uncertainty region at $t = t_i$ and let $\mathsf{UE}_{i+1} = \mathsf{UE}(x_{i+1}, y_{i+1}, a_{i+1}, b_{i+1}, \varphi_{i+1})$ be an elliptical anchor uncertainty region at $t = t_{i+1}$, with $t_i \leq t_{i+1}$. Let $v_{\max} > 0$ be a speed bound. The uncertain space-time prism*

$$\mathcal{UP}(\mathsf{UE}_i, t_i, \mathsf{UE}_{i+1}, t_{i+1}, v_{\max})$$

then consists of all spatio-temporal points $(x, y, t) \in \mathbb{R}^2 \times \mathbb{R}$ that satisfy the formula

$$\begin{aligned} \varphi_{\mathcal{UP}}(x, y, t, x_i, y_i, t_i, a_i, b_i, \varphi_i, x_{i+1}, y_{i+1}, t_{i+1}, a_{i+1}, b_{i+1}, \varphi_{i+1}, v_{\max}) := \\ t_i \leq t \leq t_{i+1} \wedge \varphi_{\mathsf{UC}^-}(x, y, t, t_i, a_i, b_i, \varphi_i, v_{\max}) \wedge \\ \varphi_{\mathsf{UC}^+}(x, y, t, t_{i+1}, a_{i+1}, b_{i+1}, \varphi_{i+1}, v_{\max}). \end{aligned}$$

□

As remarked before, because of the presence of cosines and sines, the formula of Theorem 5.2 is no longer a description in terms of polynomial inequalities. However, as soon as φ_i and φ_{i+1} are fixed, they are and we can see that $\mathcal{UP}(\mathsf{UE}_i, t_i, \mathsf{UE}_{i+1}, t_{i+1}, v_{\max})$ is a semi-algebraic set.

Based on the above theorem, we give an illustration of an space-time prism with elliptical anchor uncertainty in Figure 6. As can be seen from this figure, the rim of the uncertain prism is not located in a plane, as is the case for a classical prism.

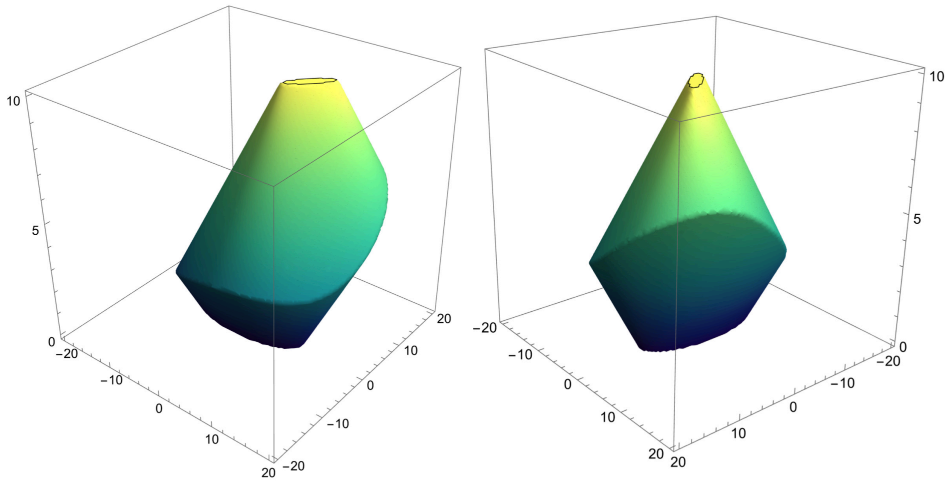

Figure 6. Two views of the space-time prism with elliptical anchor uncertainty $\mathsf{UE}_i = \mathsf{UE}(0, 0, 10, 4, 0°)$ at $t_i = 0$ and $\mathsf{UE}_{i+1} = \mathsf{UE}(6, 6, 4, 1, 45°)$ at $t_{i+1} = 10$, with $v_{\max} = 2$.

6. The potential path area of space-time prisms with elliptical anchor uncertainty regions

In this section, we study the uncertain potential path area of space-time prisms with elliptical anchor uncertainty regions. By Definition 3.4, this potential path area is the spatial projection of the uncertain prism. Therefore, we obtain a description of $\mathsf{UPPA}(\mathsf{UE}_i, t_i, \mathsf{UE}_{i+1}, t_{i+1}, v_{\max})$ by quantifying the time variable t in the formula for the prism provided by Theorem 5.2:

$$\exists t \; \varphi_{\mathcal{UP}}(x, y, t, x_i, y_i, t_i, a_i, b_i, \varphi_i, x_{i+1}, y_{i+1}, t_{i+1}, a_{i+1}, b_{i+1}, \varphi_{i+1}, v_{\max}). \tag{4}$$

However, the above formula not only contains cosines and sines but it also contains a quantifier. For membership testing and drawing the uncertain potential path area, it is desirable to have, at least, a quantifier-free expression. Even for fixed values of the angles φ_i and φ_{i+1}, symbolic quantifier-elimination software (such as provided by, for example, Mathematica) is not able to compute a quantifier-free alternative for the above expression. Also, a theoretical approach to this quantifier-elimination problem would require some kind of complicated geometric argumentation and is not obvious.

Next, we discuss how the potential path area can be visualized in general. Further, we discuss an upper bound for the uncertain potential path area and exact descriptions for a special case.

6.1. *Visualizing the uncertain potential path area of a prism with elliptical anchor uncertainty*

As an alternative, we explore the general expression of the potential path area, given by Theorem 4.2, where the potential path area is described to contain the points $p \in \mathbb{R}^2$ that satisfy

$$\bar{d}(p, \mathsf{UE}_i) + \bar{d}(p, \mathsf{UE}_{i+1}) \leq v_{\max} \cdot (t_{i+1} - t_i), \tag{5}$$

which corresponds to a "generalized ellipse" with UE_i and UE_{i+1} as foci and major axis $v_{\max} \cdot (t_{i+1} - t_i)$. To make use of this description, we would need to have an expression for the minimal distance from a point to an ellipse in the plane. But, yet again, this is not an easy problem. Calculating the distance from a point to an ellipse involves the computation of a root of a parametric polynomial of degree 4 and straightforward expression for this root is not readily available, because of which it is approximated in practical implementations using numerical methods, such as Newton's method (Eberly 2013, Uteshev and Goncharova 2018). Implementations of these approximative methods or symbolic software, such as Mathematica, that has functions implemented to express the distance to a set, allow us to use Equation (5) to produce images of the uncertain potential path area of space-time prisms with elliptical anchor uncertainty regions. Based on such implementations, Figure 7 shows the uncertain potential path area (in blue) of the uncertain prism shown in Figure 6 together with UE_i (in yellow) and UE_{i+1} (in green).

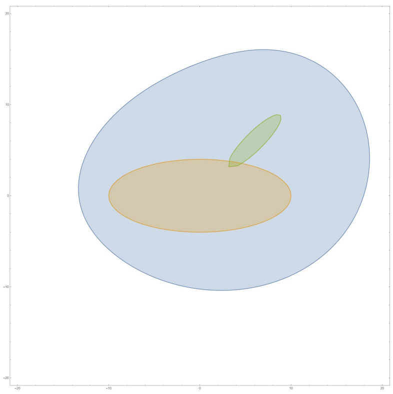

Figure 7. The uncertain potential path area of the uncertain prism shown in Figure 6.

We conclude that it is difficult to obtain an explicit description of the uncertain potential path area of space-time prisms with elliptical anchor uncertainty, although we can algorithmically visualize it. However, this potential path area can be approximated by so-called "4-ellipses". We refer the reader who is interested in this type of approximation to Appendix C, where we also discuss the quality of this approximation.

6.2. *The uncertain potential path area for circular anchor uncertainty*

When both uncertainty ellipses UE_i and UE_{i+1} are disks, it is easy to obtain an explicit description of the uncertain potential path area. This special case of our theory is already discussed by Kuijpers and Othman (2017), but the description of the uncertain potential path area is missing in that paper.

In this case, we have $\mathsf{UE}_i = D(p_i, a_i)$ and $\mathsf{UE}_{i+1} = D(p_{i+1}, a_{i+1})$ (where $D(p, \rho) = \{q \in \mathbb{R}^2 \mid d(p, q) \leq \rho\}$ denotes the closed disk with radius ρ). We can use Equation (5) and the observation that $\bar{d}(p, \mathsf{UE}_i)$ equals $d(p_i, p) - a_i$ when p is outside UE_i and equals 0 when p is inside UE_i. Using the four combinations in this observation would gives us via Equation (5) a direct and explicit description of the uncertain potential path area. However, the following theorem gives a nicer description of the uncertain potential path area as the intersection of an ellipse and two disks. We denote the ellipse with foci p_i and p_{i+1} and major axis ρ by $E^2(p_i, p_{i+1}, \rho)$.

Theorem 6.1. *Let $\mathsf{UE}_i = D(p_i, a_i)$ and $\mathsf{UE}_{i+1} = D(p_{i+1}, a_{i+1})$ be two circular uncertainty regions around p_i and p_{i+1} and with radii a_i and a_{i+1}, respectively. Then we have*

$$\begin{aligned}\mathsf{UPPA}(\mathsf{UE}_i, t_i, \mathsf{UE}_{i+1}, t_{i+1}, v_{\max}) = {} & E^2(p_i, p_{i+1}, v_{\max} \cdot (t_{i+1} - t_i) + a_i + a_{i+1}) \cap \\ & D(p_i, v_{\max} \cdot (t_{i+1} - t_i) + a_i) \cap D(p_{i+1}, v_{\max} \cdot (t_{i+1} - t_i) + a_{i+1}).\end{aligned}$$

We refer the reader who is interested in the proof of this theorem to Appendix D.

This theorem is illustrated in Figure 8, for two fixed anchor uncertainty disks and four values of $v_{\max}$. For the lowest value of $v_{\max}$ (namely, $v_{\max} = 3$), we see that the uncertain potential path area is a ellipse that is truncated at both sides, whereas for higher values of $v_{\max}$ (namely, $v_{\max} = 4$ and 5) we already have that UE_i belongs to the ellipse. For the highest value $v_{\max} = 8$, both UE_i and UE_{i+1} are contained in the ellipse.

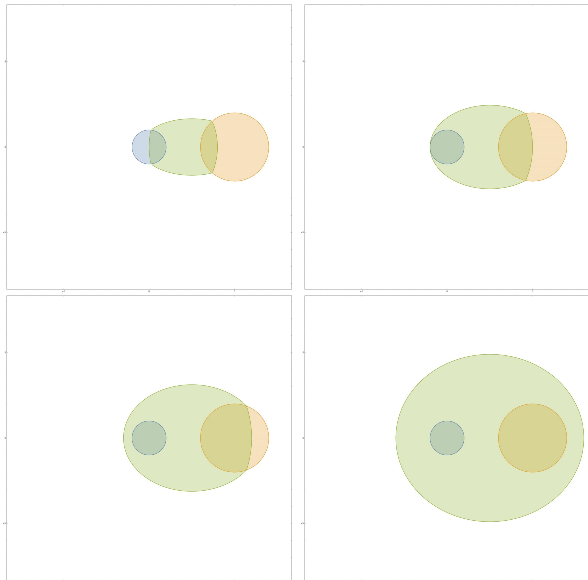

Figure 8. For $\mathsf{UE}_i = D((0, 0), 1)$ (in blue) and $\mathsf{UE}_{i+1} = D((5, 0), 2)$ (in red), $t_i = 0$ and $t_{i+1} = 1$, we show $\mathsf{UPPA}(\mathsf{UE}_i, t_i, \mathsf{UE}_{i+1}, t_{i+1}, v_{\max})$ for $v_{\max} = 3, 4, 5$ and 8, respectively.

7. Some application scenarios

In this section, we present some application scenarios, in which we illustrate the usefulness of our results on space-time prisms and their potential path areas when anchor uncertainty is given by elliptical regions. Our example is in the spirit of the work by McClintock *et al.* (2015) who have used Argos-based data in their study of two types of seals. This Argos data consists of location fixes accompanied by location error ellipses and in their work these data are the basis for the analysis of animal behavior. To avoid getting entangled in biological details, we work with a synthetic dataset consisting of five fixes of an imaginary sea animal given in local (x, y) coordinates together with their error ellipses, which are given by a triple of major and minor axes and an orientation angle (a, b, φ), as described above. Our toy dataset is given in Table 1 (where spatial and temporal units are irrelevant, since we only want to illustrate the principles).

time t	location (x, y)	ellipse (a, b, φ)
0	$(0, 0)$	$(1, 3, 45°)$
5	$(5, -8)$	$(1, 2, 0°)$
10	$(12, 0)$	$(3, 1, 25°)$
15	$(15, 5)$	$(2, \frac{1}{2}, 0°)$
20	$(15, 10)$	$(1, 1, 0°)$

Table 1. Synthetic dataset of five uncertain elliptical anchors of an imaginary sea animal.

In the work of McClintock *et al.* (2015), these data would be visualized as depicted in Figure 9: the error ellipses around the location fixes, accompanied by a polyline that represents the spatial projection of the linear interpolation trajectory between these anchors. This polyline is a purely spatial object and it corresponds to the spatial projection of the trajectory of minimal speed between the consecutive anchor points. As such, it gives little information on the locations that our sea animal might have visited.

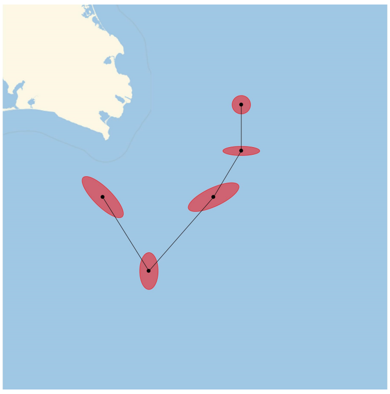

Figure 9. Visualisation of the spatial projection of the dataset of Table 1 with the error ellipses (in red) and the linear interpolation between consecutive location fixes (in black).

Using the results developed in this paper, we can take a step towards gaining more insight in the potential movement of the sea animal. Obviously, in our context, we need to assume some maximal speed. This could be a speed bound know by biologists for this particular type of animal, but it can be any other meaningful quantity. In our example, we have taken the value for $v_{\max}$ to be twice the minimal speed of the animal between any two consecutive anchors. For this choice of speed limits, we depict the uncertain potential path area for the given elliptical anchor uncertainty regions in Figure 10. The respective uncertain potential path areas are shown there in yellow, blue, green and red (in increasing temporal order). This picture gives us an idea of the locations the animal might have visited and from yellow potential path area, we can derive that it is possible the animal might have been at the coast line.

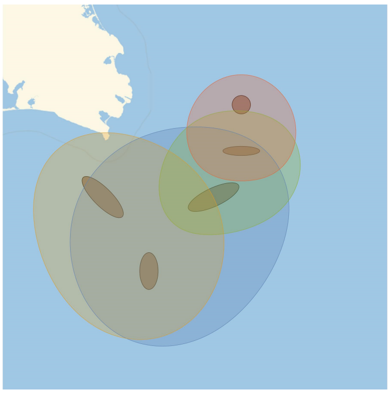

Figure 10. Visualisation of the uncertain potential path areas, given the fixes and their error ellipses of Table 1.

Next, we can add the temporal dimension and depict the chain of uncertain space-time prisms corresponding to the five measured locations of this animal. This information is shown in Figure 11.

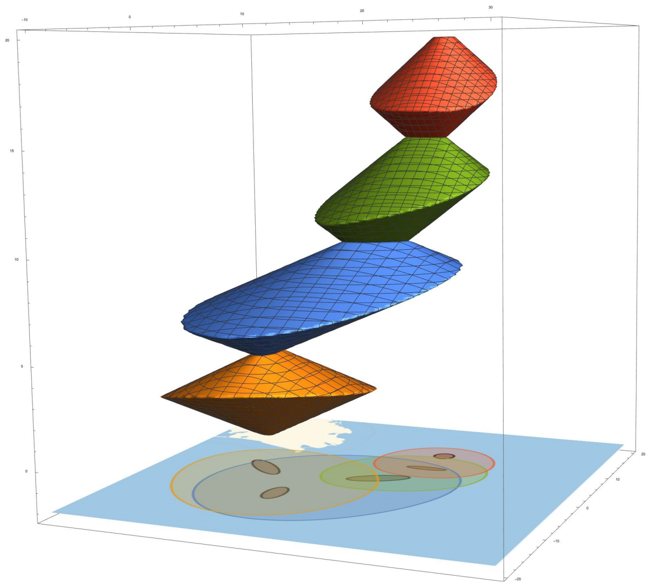

Figure 11. Visualisation of the chain of space-time prisms, given the fixes and their error ellipses of Table 1.

To conclude this section, we present another example, in line with the previous one, but involving two animals. Both animals have four location fixes with error ellipses (we omit the details) and these are depicted in orange and green, respectively, in Figure 12 on the left together with the respective linear interpolation trajectories. When a biologist who knows the maximal speed of these animals would depict their corresponding uncertain potential path areas (as shown in Figure 12 on the right), s/he sees that there is an overlapping area between these spatial sets. This might be an indication that these animals have met. We remark that meeting or not meeting of animals is of interest in the study of how infectious diseases spread. However, a closer inspection, using the full spatio-temporal information given by their chains of space-time prisms shows that these chains do not intersect. These chains are shown in Figure 13. These animals have actually visited the same area but at different moments in time.

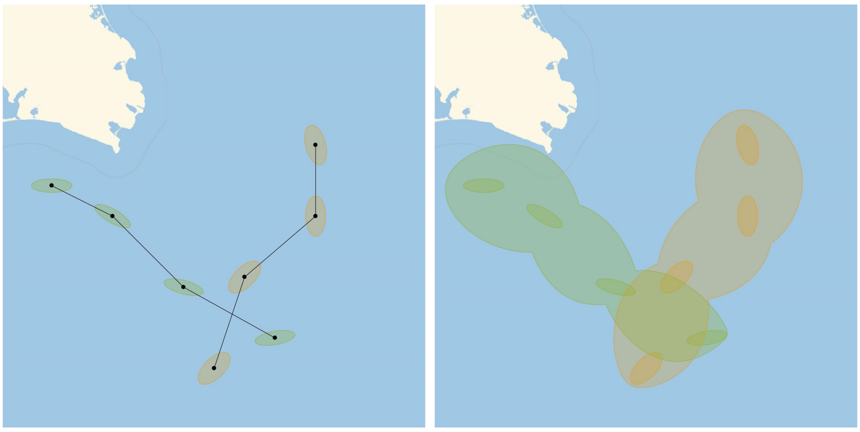

Figure 12. Visualisation of the data of two animals (on the left) and the corresponding uncertain potential path areas (on the right).

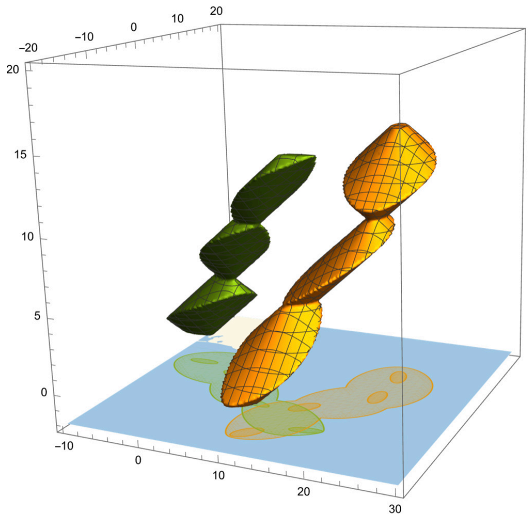

Figure 13. The chains of prisms of the two animals of Figure 12.

8. Conclusion and discussion

We investigate the geometry of space-time prisms and their potential path areas in the setting where the prism anchors have a spatial uncertainty area attached to them. Our main result gives a characterisation of such space-time prisms and their potential path areas in terms of a generalised distance function between closed subsets of the ambient space. A major part of this paper is devoted to the application of this general result to the case where the anchor uncertainty regions are ellipses. We have seen that an explicit (that is, quantifier-free) description of the uncertain prisms is quite hard to obtain and that it uses polynomials of degree eight whereas classical prims can be described by quadratic polynomials. From a geometric point of view, these uncertain prisms are therefore complicated to handle and a study of, for example, the "alibi query" (Grimson *et al.* 2011) (which amounts to deciding prism intersection) is quite infeasible. Therefore, moving from anchor uncertainty disks (as addressed by Kuijpers and Othman (2017)) to ellipses is quite a leap and, in practice, uncertainty disks may be more desirable than uncertainty ellipses. Also, a description of the uncertain potential path areas is difficult to obtain when anchor uncertainty is modelled by ellipses. Here, the difficulty is that an explicit formula for the distance between a point and an ellipse is problematic.

We conclude by remarking that elliptical anchor uncertainty regions are just one example. We used this example for its practical relevance and to show that this relevant case can easily lead to complicated geometry. However, other application domains might require other shapes of uncertainty regions. For example, in the context of location fixes produced using a mobile phone antenna, the uncertainty regions might be parts of a pie-shaped region (depending on signal intensity and direction of the antenna). When locations are hand-recorded, they might take the shape of some building that could be modelled by polygonal shapes. In many application, it might be useful and sufficient to work with polygons, which might also serve as approximations of more complicated regions. Our general result can be applied straightforwardly in the case of convex polygons and this can be a useful substitute for the case of ellipses that can be arbitrarily approximated by polygonal regions. The example of polygons may suffice for many practical applications and we leave it for further study.

Disclosure statement

The authors report there are no competing interests to declare.

Funding

The research of Arthur Jansen was supported by the Bijzonder Onderzoeksfonds (BOF) from UHasselt with reference BOF22OWB06.

Notes on contributor(s)

Both authors contributed equally to the research and the writing.

Data and codes availability statement

No data was used in this research. The Mathematica code (including the parameter setting) to produce most of the figures is available via the link: https://doi.org/10.6084/m9.figshare.25020620

References

Argos, 2018. The argos tracking system. www.argos-system.org.

Bochnak, J., Coste, M., and Roy, M.F., 1998. *Real algebraic geometry.* Ergebnisse der Mathematik und ihrer Grenzgebiete, vol. 36. Springer-Verlag.

Burns, L., 1979. *Transportation, temporal, and spatial components of accessibility.* Lexington, MA: Lexington Books.

Chen, B., Lam, W., and Sumalee, A., 2013. Reliable space-time prism under travel time uncertainty. *Annals of the Association of American Geographers*, 103, 1502–1521.

Delafontaine, M., Neutens, T., and van de Weghe, N., 2011. Modelling potential movement in constrained travel environments using rough space-time prisms. *International Journal of Geographical Information Science*, 25, 1389–1411.

Eberly, D., 2013. Distance from a point to an ellipse, an ellipsoid, or a hyper-ellipsoid. Available from: `https://www.geometrictools.com/Documentation/DistancePointEllipseEllipsoid.pdf`.

Egenhofer, M., 2003. Approximation of geopatial lifelines. *In*: *SpadaGIS, Workshop on Spatial Data and Geographic Information Systsems.* Electr. proceedings, 4p.

Giannotti, F. and Pedreschi, D., eds., 2008. *Mobility, Data Mining and Privacy - Geographic Knowledge Discovery.* Springer.

Gray, A., 1997. *Modern differential geometry of curves and surfaces with mathematica.* CRC Press, Boca Raton, FL. (Second edition).

Grimson, R., Kuijpers, B., and Othman, W., 2011. An analytic solution to the alibi query in the space-time prisms model for moving object data. *International Journal of Geographical Information Science*, 25 (2), 293–322.

Güting, R. and Schneider, M., 2005. *Moving object databases.* Morgan Kaufmann.

Hägerstrand, T., 1970. What about people in regional science? *Papers of the Regional Science Association*, 24, 7–21.

Jacquez, G.M., 2000. Spatial analysis in epidemiology: Nascent science or a failure of gis? *Journal of Geographical Systems*, 2 (1), 91–97.

Jacquez, G.M., Greiling, D.A., and Kaufmann, A.M., 2005. Design and implementation of a space-time intelligence system for disease surveillance. *Journal of Geographical Systems*, 7 (1), 7–23.

Kaplan, E. and Hegarty, C., 2017. *Understanding GPS/GNSS: Principles and applications.* Artech House Publishers, London. (3rd Edition).

Kubrusly, C. and Conci, A., 2017. Distance between sets – a survey. *Advances in Mathematical Sciences and Applications*, 26, 1–18.

Kuijpers, B. and Othman, W., 2009. Modelling uncertainty of moving objects on road networks via space-time prisms. *International Journal of Geographical Information Science*, 23, 1095–1117.

Kuijpers, B., *et al.*, 2010. Anchor uncertainty and space-time prisms on road networks. *International Journal of Geographical Information Science*, 24 (8), 1223–1248.

Kuijpers, B. and Othman, W., 2010. Trajectory databases: Data models, uncertainty and complete query languages. *Journal of Computer and System Sciences*, 76 (7), 538–560.

Kuijpers, B. and Othman, W., 2017. The geometry of space-time prisms with uncertain anchors. *Int. J. Geogr. Inf. Sci.*, 31 (9), 1722–1748. Available from: `https://doi.org/10.1080/13658816.2017.1319950`.

Kwan, M.P. and Hong, X.D., 1998. Network-based constraints-oriented choice set formation using GIS. *Journal of Geographical Systems*, 5, 139–162.

Kwan, M.P., 1999. Gender and individual access to urban opportunities: A study using space-time measures. *The Professional Geographer*, 51 (2), 211–227. Available from: `http://dx.doi.org/10.1111/0033-0124.00158`.

Lenntorp, B., 1976. *Paths in space-time environments: A time-geographic study of the movement possibilities of individuals.* No. 44 in Series B. Lund Studies in Geography.

Liao, F., Rasouli, S., and Timmermans, H., 2014. Incorporating activity-travel time uncertainty and stochastic space-time prisms in multi-state supernetworks for activity-travel scheduling. *International Journal of Geographic Information Science*, 28, 928–945.

Löytönen, M., 1998. Gis, time geography and health. *In*: A. Gatrell and M.e. Löytönen, eds.

Location-based services. London, UK: Taylor and Francis, 97–110.
Maxwell, J.C., 1845. On the description of oval curves, and those having a plurality of foci; with remarks by Professor Forbes. *Proceedings of the Royal Society of Edinburgh*, 2 (28), 89–91.
McClintock, B.T., *et al.*, 2015. Modelling animal movement using the argos satellite telemetry location error ellipse. *Methods in Ecology and Evolution*, 6, 266–277.
Miller, H.J., 2005a. Necessary space - time conditions for human interaction. *Environment and Planning B: Planning and Design*, 32 (3), 381–401.
Miller, H., 1991. Modeling accessibility using space-time prism concepts within geographical information systems. *International Journal of Geographical Information Systems*, 5, 287–301.
Miller, H., 2005b. A measurement theory for time geography. *Geographical Analysis*, 37 (1), 17–45.
Nie, J., Parrilo, P.A., and Sturmfels, B., 2008. Semidefinite representation of the k-ellipse. *In*: *Algorithms in algebraic geometry*. Springer New York, 117–132. Available from: `https://doi.org/10.1007%2F978-0-387-75155-9_7`.
Ochkov, V., *et al.*, 2019. A new ellipse or math porcelain service. *Symmetry*, 11 (2), 184. Available from: `https://doi.org/10.3390/sym11020184`.
Othman, W., 2009. *Uncertainty management in trajectory databases*. Thesis (PhD). Hasselt University.
Paredaens, J., Kuper, G., and Libkin, L., eds., 2000. *Constraint databases*. Springer-Verlag.
Patterson, Z. and Farber, S., 2015. Potential path areas and activity spaces in application: A review. *Transport Reviews*, 35 (6), 679–700. Available from: `http://dx.doi.org/10.1080/01441647.2015.1042944`.
Pfoser, D., Tryfona, N., and C., J., 2005. Indeterminacy and spatiotemporal data: Basic definitions and case study. *Geoinformatica*, 9 (3), 211–236.
Ratcliffe, J.H., 2006. A temporal constraint theory to explain opportunity-based spatial offending patterns. *Journal of Research in Crime and Delinquency*, 43, 261–291.
Timmermans, H., Arentze, T., and Joh, C., 2002. Analysing space-time behaviour: new approaches to old problems. *Progress in human geography*, 26 (2), 175–190.
Trajcevski, G., *et al.*, 2004. Managing uncertainty in moving objects databases. *ACM Trans. Database Syst.*, 29 (3), 463–507.
Uteshev, A.Y. and Goncharova, M.V., 2018. Point-to-ellipse and point-to-ellipsoid distance equation analysis. *J. Comput. Appl. Math.*, 328, 232–251. Available from: `https://doi.org/10.1016/j.cam.2017.07.021`.
Weisstein, E.W., 2023. Ellipse parallel curves. Available from: `https://mathworld.wolfram.com/EllipseParallelCurves.html`.
WoframAlpha, 2023. Ellipse parallel curves. Available from: `https://www.wolframalpha.com/input/?i=ellipse+parallel+curves`.
Wolfson, O., 2002. Moving objects information management: The database challenge. *In*: *Proceedings of the 5th Intl. Workshop Next Generation Information Technologies and Systems*. Springer, 75–89.
Wu, Y.H. and Miller, H., 2002. Computational tools for measuring space-time accessibility within transportation networks with dynamic flow. *Journal of Transportation and Statistics*, 4 (2/3), 1–14.
Yu, H. and Shaw, S.L., 2008. Exploring potential human activities in physical and virtual spaces: a spatio-temporal GIS approach. *Int. J. Geogr. Inf. Sci.*, 22 (4), 409–430.

Appendix A. An expression for $\mathsf{Toroid}(x, y, a, b, d)$

From (WoframAlpha 2023), we have the following expression for $\mathsf{Toroid}(x, y, a, b, d)$:

$$
\begin{aligned}
&\mathsf{Toroid}(x,y,a,b,d) = \\
&b^4x^8 + 2b^6x^6 + 2y^2b^4x^6 - 4a^2b^4x^6 + 2y^2a^2b^2x^6 - 4b^4d^2x^6 + 2a^2b^2d^2x^6 + b^8x^4 - 2y^2b^6x^4 - 6a^2b^6x^4 \\
&+ y^4a^4x^4 + y^4b^4x^4 + 6a^4b^4x^4 + 2y^2a^2b^4x^4 + a^4d^4x^4 + 6b^4d^4x^4 - 6a^2b^2d^4x^4 - 6y^2a^4b^2x^4 \\
&+ 4y^4a^2b^2x^4 - 6b^6d^2x^4 - 2y^2a^4d^2x^4 - 6y^2b^4d^2x^4 + 10a^2b^4d^2x^4 - 6a^4b^2d^2x^4 + 2y^2a^2b^2d^2x^4 \\
&- 2a^2b^8x^2 - 2y^4a^6x^2 + 6a^4b^6x^2 + 6y^2a^2b^6x^2 - 2a^4d^6x^2 - 4b^4d^6x^2 + 6a^2b^2d^6x^2 + 2y^6a^4x^2 \\
&- 4a^6b^4x^2 - 10y^2a^4b^4x^2 - 6y^4a^2b^4x^2 - 2a^6d^4x^2 + 6b^6d^4x^2 + 6y^2a^4d^4x^2 + 6y^2b^4d^4x^2 - 8a^2b^4d^4x^2 \\
&+ 4a^4b^2d^4x^2 - 10y^2a^2b^2d^4x^2 + 6y^2a^6b^2x^2 + 2y^4a^4b^2x^2 + 2y^6a^2b^2x^2 - 2b^8d^2x^2 \\
&+ 4y^2a^6d^2x^2 + 4y^2b^6d^2x^2 + 4a^2b^6d^2x^2 - 6y^4a^4d^2x^2 - 2y^4b^4d^2x^2 - 8a^4b^4d^2x^2 \\
&- 6y^2a^2b^4d^2x^2 + 6a^6b^2d^2x^2 - 6y^2a^4b^2d^2x^2 + 2y^4a^2b^2d^2x^2 + y^4a^8 + a^4b^8 + a^4d^8 \\
&+ b^4d^8 - 2a^2b^2d^8 + 2y^6a^6 - 2a^6b^6 - 4y^2a^4b^6 - 2a^6d^6 - 2b^6d^6 - 4y^2a^4d^6 - 2y^2b^4d^6 \\
&+ 2a^2b^4d^6 + 2a^4b^2d^6 + 6y^2a^2b^2d^6 + y^8a^4 + a^8b^4 + 6y^2a^6b^4 + 6y^4a^4b^4 + a^8d^4 + b^8d^4 \\
&+ 6y^2a^6d^4 - 2y^2b^6d^4 + 2a^2b^6d^4 + 6y^4a^4d^4 + y^4b^4d^4 - 6a^4b^4d^4 + 4y^2a^2b^4d^4 + 2a^6b^2d^4 \\
&- 8y^2a^4b^2d^4 - 6y^4a^2b^2d^4 - 2y^2a^8b^2 - 6y^4a^6b^2 - 4y^6a^4b^2 - 2y^2a^8d^2 - 2a^2b^8d^2 - 6y^4a^6d^2 \\
&+ 2a^4b^6d^2 + 6y^2a^2b^6d^2 - 4y^6a^4d^2 + 2a^6b^4d^2 - 8y^2a^4b^4d^2 - 6y^4a^2b^4d^2 \\
&- 2a^8b^2d^2 + 4y^2a^6b^2d^2 + 10y^4a^4b^2d^2 + 2y^6a^2b^2d^2
\end{aligned}
$$

Appendix B. A proof of Theorem 5.1

In this appendix, we give the details of the proof of Theorem 5.1, for the interested reader. In order to prove this theorem, we need some terminology and a lemma. Let UE_i and $v_{\max} > 0$ be as in the statement of the theorem. We abbreviate $v_{\max} \cdot (t - t_i)$, which is $v_{\max} \cdot t$ in this setting, by δ_t to contain the length of the expressions.

Our aim is to find a quantifier-free expression (that is, a Boolean combination of polynomial inequalities) for the bottom cone, that can be seen as consisting of the sets

$$\mathsf{C}_t := \{p \in \mathbb{R}^2 \times \mathbb{R} \mid \exists q \in \mathbb{R}^2 : q \in \mathsf{UE}_i \wedge d(p,q) \leq \delta_t\},$$

for all $t \geq t_i = 0$. The description that we have just given of C_t contains an existential quantifier and our aim is to find a quantifier-free alternative. In order to achieve this, we show that the set C_t is the union of three sets, and we give a quantifier-free description of each of these sets.

The first of these three sets is simply UE_i and we know it is described by the quantifier-free inequality $x^2/a_i^2 + y^2/b_i^2 \leq 1$, which is independent of t.

We denote the second of these three sets by TR_t and we define it to be the region between the inner and outer parallel curves of UE_i with offset δ_t and $-\delta_t$. We already know that TR_t is described by the quantifier-free polynomial inequality $\mathsf{Toroid}(x, y, a_i, b_i, \delta_t) \leq 0$.

We remark that TR_t is enclosed by the outer parallel curve of $\partial\mathsf{UE}_i$ at offset δ_t. This means that $\mathsf{TR}_t \subseteq \mathsf{C}_t$. We denote by ITR_t the set $\mathsf{C}_t \setminus \mathsf{TR}_t$. This is the the region enclosed by the inner parallel curve of $\partial\mathsf{UE}_i$ with offset $-\delta_t$.

To describe the the third set, we first define the line segment $\mathsf{L} = \{(x, 0) \in \mathbb{R}^2 \mid -a \leq x \leq a\}$ and then define the region the region L_t as $\{p \in \mathbb{R}^2 \mid \exists q \in \mathsf{L} : d(p, q) \leq \delta_t\}$. This is the set of all points at distance at most δ_t from the line segment L and it is easy to see that it corresponds to the set

$$\{(x,y) \in \mathbb{R}^2 \mid (-a \leq x \leq a \wedge -\delta_t \leq y \leq \delta_t) \vee (x+a)^2 + y^2 \leq \delta_t^2 \vee (x-a)^2 + y^2 \leq \delta_t^2\},$$

which is given by a quantifier-free formula.

Figure B1 illustrates the region L_t for the situation described in the top two images in Figure 5.

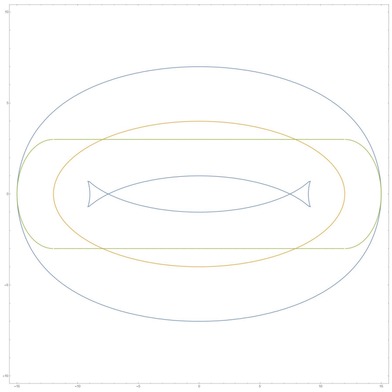

Figure B1. For the top left figure in Figure 5, this figure gives the bordering curve of the region L_t in green.

With the above terminology, we are ready to prove the following lemma.

Lemma B.1. *Using the above notation, we have the inclusion* $\mathsf{ITR}_t \subseteq L_t \cup \mathsf{UE}_i$.

Proof of Lemma B.1. Because ITR_t is the region enclosed by the inner parallel curve, it is enough to show that every point of the inner parallel curve is included in $\mathsf{L}_t \cup \mathsf{UE}_i$. Say point p is a point on the inner parallel curve of $\partial\mathsf{UE}_i$ with offset δ_t. If $p \in \mathsf{UE}_i$, then we are done. So, let us assume that $p \notin \mathsf{UE}_i$. Because p is a point on the inner parallel curve, there exists a point $q = (x_q, y_q) \in \partial\mathsf{UE}_i$, such that p lies on the normal on $\partial\mathsf{UE}_i$ at q. The normal of $\partial\mathsf{UE}_i$ at q is given by the equation $a_i^2 y_q(x_q - x) = b_i^2 x_q(y_q - y)$. To find the intersection of the normal with the x-axis, we fill in $y = 0$ and obtain $x_i = x_q\frac{a_i^2-b_i^2}{a_i^2}$. Because $q \in \partial\mathsf{UE}_i$, we have $-a_i \leq x_q \leq a_i$, and because $a_i \geq b_i$, we have $0 \leq \frac{a_i^2-b_i^2}{a_i^2} \leq 1$. Combining these two gives us $-a_i \leq x_i \leq a_i$, which means that $(x_i, 0) \in \mathsf{L}_t$. Now, because $(x_i, 0)$ lies inside the ellipse and p lies outside the ellipse, $(x_i, 0)$ must lie between p and q. Since $d(p,q) = \delta_t$ (by definition of the parallel curve), $d(p,(x_i,0)) \leq \delta_t$ which means $p \in \mathsf{L}_t$. This completes the proof. $\square$

Using this lemma, we can now finish the proof of the theorem.

Proof of Theorem 5.1. To prove the theorem, what remains to be shown is the set equality $\mathsf{C}_t = \mathsf{TR}_t \cup \mathsf{L}_t \cup \mathsf{UE}_i$. Indeed, before we have already presented quantifier-free formulas for each of these sets.

We first show that $\mathsf{C}_t \subseteq \mathsf{TR}_t \cup \mathsf{L}_t \cup \mathsf{UE}_i$. If $p \in \mathsf{C}_t$, then either $p \in \mathsf{TR}_t$ or $p \in \mathsf{ITR}_t$, by definition of ITR_t. In the first case, the inclusion is clear. For the second case, we obtain $p \in \mathsf{L}_t \cup \mathsf{UE}_i$ by Lemma B.1. So, we have shown $p \in \mathsf{TR}_t \cup \mathsf{L}_t \cup \mathsf{UE}_i$.

For the inclusion $\mathsf{TR}_t \cup \mathsf{L}_t \cup \mathsf{UE}_i \subseteq \mathsf{C}_t$, we already know that $\mathsf{TR}_t \subseteq \mathsf{C}_t$. And it is trivial that $\mathsf{UE}_i \subseteq \mathsf{C}_t$. What is left to prove is $\mathsf{L}_t \subseteq \mathsf{C}_t$, but this follows directly from the fact that $\mathsf{L} \subseteq \mathsf{UE}_i$. This finishes the proof. $\square$

Appendix C. Approximating the uncertain potential path area using 4-ellipses

In this appendix, we show how the uncertain potential path area can be approximated by "4-ellipses" and we discuss the quality of this approximation.

When $(x_i, y_i, t_i), (x_{i+1}, y_{i+1}, t_{i+1}) \in \mathbb{R}^2 \times \mathbb{R}$ are two anchor points with elliptical uncertainty areas $\mathsf{UE}_i = \mathsf{UE}(x_i, y_i, t_i, a_i, b_i, \varphi_i)$ and $\mathsf{UE}_{i+1} = \mathsf{UE}(x_{i+1}, y_{i+1}, t_{i+1}, a_{i+1}, b_{i+1}, \varphi_{i+1})$, then we denote the foci of the ellipse $\partial\mathsf{UE}_i$ by f_i and f'_i and the foci of the ellipse $\partial\mathsf{UE}_{i+1}$ by f_{i+1} and f'_{i+1}. The theorem below gives an upper bound for the uncertain potential path area in terms of the four foci of these two ellipses and their major axes a_i and a_{i+1}. This upper bound is delimited by a so-called "4-ellipse". We first define this notion. Given four points a, b, c and d in the plane $\mathbb{R}^2$, the *filled 4-ellipse with foci a, b, c and d and "diameter" $\rho > 0$*, denoted $E^4(a, b, c, d, \rho)$, consists of all points $p \in \mathbb{R}^2$ for which

$$d(a, p) + d(b, p) + d(c, p) + d(d, p) \leq \rho.$$

When we replace the inequality symbol with an equality symbol in the above equation, we obtain a description of the border $\partial E^4(a, b, c, d, \rho)$, which we call the *4-ellipse with foci a, b, c and d and diameter ρ*. We remark that 4-ellipses belong to a family of generalised ellipses, called n-ellipses. They were studied by James Clerk Maxwell (at the age of 14) in 1845 (Maxwell 1845), who improved the their description compared to the one first given by René Descartes in the 17th century. We remark that, for n even, the algebraic degree of an n-ellipse is $2^n - \binom{n}{n/2}$ (Nie *et al.* 2008), which means that the degree of a 4-ellipse is 10.

The following theorem shows uncertain potential path area can be approximated (from above) by 4-ellipses.

Theorem C.1. *Let UE_i and UE_{i+1} be two elliptical uncertainty areas with foci f_i, f'_i and f_{i+1}, f'_{i+1} and semi-major axes a_i and a_{i+1}, respectively (as described above). Then we have*

$$\begin{aligned}&\mathsf{UPPA}(x_i, y_i, t_i, a_i, b_i, \varphi_i, x_{i+1}, y_{i+1}, t_{i+1}, a_{i+1}, b_{i+1}, \varphi_{i+1}, v_{\max})\\ &\qquad\subseteq E^4(f_i, f'_i, f_{i+1}, f'_{i+1}, 2a_i + 2a_{i+1} + 2v_{\max} \cdot (t_{i+1} - t_i)).\end{aligned}$$

Before proving Theorem C.1, we need the following lemma.

Lemma C.2. *Let UE_i be an elliptical anchor uncertainty region (as above) and let p be a spatial point. Then $2 \cdot \bar{d}(p, \mathsf{UE}_i) \leq d(p, f_i) + d(p, f'_i) + 2a_i$.*

Proof. Let q be the point in UE_i with minimal distance to p, that is, $d(p, q) = \bar{d}(p, \mathsf{UE}_i)$. We remark that because of the convexity of UE_i, this point q is unique. If p lies inside UE_i, then $\bar{d}(p, \mathsf{UE}_i) = 0$ and the conclusion certainly holds. So, we assume that $p \notin \mathsf{UE}_i$, which implies that q lies on the border of UE_i. Applying the triangle inequality, we obtain $d(p, q) \leq d(p, f_i) + d(f_i, q)$, as well as $d(p, q) \leq d(p, f'_i) + d(f'_i, q)$. Combining these two inequalities gives $2 \cdot d(p, q) \leq d(p, f_i) + d(f_i, q) + d(p, f'_i) + d(f'_i, q)$. By using the fact that q lies on the border of UE_i, and thus $d(q, f_i) + d(q, f'_i) = 2a_i$, and the assumption that $d(p, q) = \bar{d}(p, \mathsf{UE}_i)$, we obtain the desired inequality $2 \cdot \bar{d}(p, \mathsf{UE}_i) \leq d(p, f_i) + d(p, f'_i) + 2a_i$. □

Using the above lemma for UE_i and UE_{i+1}, we can prove Theorem C.1.

Proof of Theorem C.1 Lemma C.4 gives us the two inequalities $2 \cdot \bar{d}(p, \mathsf{UE}_i) \le d(p, f_i) + d(p, f_i') + 2a_i$ and $2 \cdot \bar{d}(p, \mathsf{UE}_{i+1}) \le d(p, f_{i+1}) + d(p, f_{i+1}') + 2a_{i+1}$. Adding these two inequalities gives $2 \cdot (\bar{d}(p, \mathsf{UE}_i) + \bar{d}(p, \mathsf{UE}_{i+1}) - a_i - a_{i+1}) \le d(p, f_i) + d(p, f_i') + d(p, f_{i+1}) + d(p, f_{i+1}')$. By the assumption that p lies in the 4-ellipse with foci f_i, f_i', f_{i+1} and f_{i+1}' and diameter $2a_i + 2a_{i+1} + 2v_{\max} \cdot (t_{i+1} - t_i)$, we have $d(p, f_i) + d(p, f_i') + d(p, f_{i+1}) + d(p, f_{i+1}') \le 2a_i + 2a_{i+1} + 2v_{\max} \cdot (t_{i+1} - t_i)$, and thus $2 \cdot (\bar{d}(p, \mathsf{UE}_i) + \bar{d}(p, \mathsf{UE}_{i+1}) - a_i - a_{i+1}) \le 2a_i + 2a_{i+1} + 2v_{\max} \cdot (t_{i+1} - t_i)$. We conclude the proof by simple manipulation of the above inequality to obtain $\bar{d}(p, \mathsf{UE}_i) + \bar{d}(p, \mathsf{UE}_{i+1}) \le 2a_i + 2a_{i+1} + v_{\max} \cdot (t_{i+1} - t_i)$. $\square$

We illustrate the above theorem by showing, in Figure C1, the uncertain potential path area of the uncertain prism shown in Figure 6 together with the 4-ellipse that contains it.

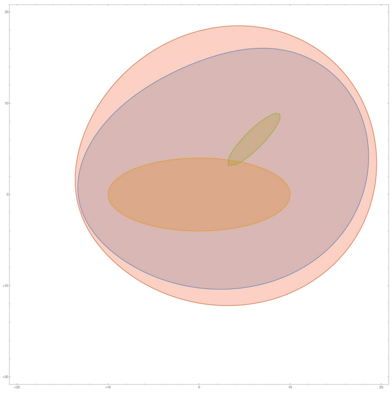

Figure C1. The uncertain potential path area of the uncertain prism shown in Figure 6 together with the larger 4-ellipse in red.

We proceed by showing the quality of this overestimation of the uncertain potential path area by a 4-ellipse, in the next theorem.

Theorem C.3. *Let UE_i and UE_{i+1} be elliptical anchor uncertainty ellipses with foci f_i, f_i' and f_{i+1}, f_{i+1}' and long axes a_i and a_{i+1}, respectively (as described above). Let $v_{\max} > 0$ be a speed bound. Then, for every point p in $E^4(f_i, f_i', f_{i+1}, f_{i+1}', 2a_i + 2a_{i+1} + 2v_{\max} \cdot (t_{i+1} - t_i))$, we have*

$$\bar{d}(p, \mathsf{UE}_i) + \bar{d}(p, \mathsf{UE}_{i+1}) \le 2a_i + 2a_{i+1} + v_{\max} \cdot (t_{i+1} - t_i).$$

Before proving Theorem C.3, we need the following lemma.

Lemma C.4. *Let UE_i be an elliptical anchor uncertainty region (as above) and let p be a spatial point. Then $2 \cdot \bar{d}(p, \mathsf{UE}_i) \le d(p, f_i) + d(p, f_i') + 2a_i$.*

Proof. Let q be the point in UE_i with minimal distance to p, that is, $d(p, q) = \bar{d}(p, \mathsf{UE}_i)$. We remark that because of the convexity of UE_i, this point q is unique. If p lies inside UE_i, then $\bar{d}(p, \mathsf{UE}_i) = 0$ and the conclusion certainly holds. So, we assume that $p \notin \mathsf{UE}_i$, which implies that q lies on the border of UE_i. Applying the triangle inequality, we obtain $d(p, q) \le d(p, f_i) + d(f_i, q)$, as well as $d(p, q) \le d(p, f_i') + d(f_i', q)$. Combining these two inequalities gives $2 \cdot d(p, q) \le d(p, f_i) + d(f_i, q) + d(p, f_i') + d(f_i', q)$. By using the fact that q lies on the border of UE_i, and thus $d(q, f_i) + d(q, f_i') = 2a_i$, and the assumption that $d(p, q) = \bar{d}(p, \mathsf{UE}_i)$, we obtain the desired inequality $2 \cdot \bar{d}(p, \mathsf{UE}_i) \le$

$d(p, f_i) + d(p, f'_i) + 2a_i$. □

Using the above lemma for UE_i and UE_{i+1}, we can prove Theorem C.3.

Proof of Theorem C.3 Lemma C.4 gives us the two inequalities $2 \cdot \bar{d}(p, \mathsf{UE}_i) \leq d(p, f_i) + d(p, f'_i) + 2a_i$ and $2 \cdot \bar{d}(p, \mathsf{UE}_{i+1}) \leq d(p, f_{i+1}) + d(p, f'_{i+1}) + 2a_{i+1}$. Adding these two inequalities gives $2 \cdot (\bar{d}(p, \mathsf{UE}_i) + \bar{d}(p, \mathsf{UE}_{i+1}) - a_i - a_{i+1}) \leq d(p, f_i) + d(p, f'_i) + d(p, f_{i+1}) + d(p, f'_{i+1})$. By the assumption that p lies in the 4-ellipse with foci f_i, f'_i, f_{i+1} and f'_{i+1} and diameter $2a_i + 2a_{i+1} + 2v_{\max} \cdot (t_{i+1} - t_i)$, we have $d(p, f_i) + d(p, f'_i) + d(p, f_{i+1}) + d(p, f'_{i+1}) \leq 2a_i + 2a_{i+1} + 2v_{\max} \cdot (t_{i+1} - t_i)$, and thus $2 \cdot (\bar{d}(p, \mathsf{UE}_i) + \bar{d}(p, \mathsf{UE}_{i+1}) - a_i - a_{i+1}) \leq 2a_i + 2a_{i+1} + 2v_{\max} \cdot (t_{i+1} - t_i)$. We conclude the proof by simple manipulation of the above inequality to obtain $\bar{d}(p, \mathsf{UE}_i) + \bar{d}(p, \mathsf{UE}_{i+1}) \leq 2a_i + 2a_{i+1} + v_{\max} \cdot (t_{i+1} - t_i)$. □

Appendix D. A proof of Theorem 6.1

In this appendix, we give the details of the proofs of Theorem 6.1, for the interested reader.

Proof of Theorem 6.1 For the equality in the statement of the theorem, we abbreviate $\mathsf{UPPA}(\mathsf{UE}_i, t_i, \mathsf{UE}_{i+1}, t_{i+1}, v_{\max})$ by UPPA, the ellipse by E^2 and the disks, centered at p_i and p_{i+1} by D_i and D_{i+1}, respectively.

To prove the inclusion $\mathsf{UPPA} \subseteq E^2 \cap D_i \cap D_{i+1}$, we take p to be be a point in UPPA. This means that $\bar{d}(p, \mathsf{UE}_i) + \bar{d}(p, \mathsf{UE}_{i+1}) \leq v_{\max} \cdot (t_{i+1} - t_i)$. Because UE_i and UE_{i+1} are disks, we have $\bar{d}(p, \mathsf{UE}_i) \geq d(p, p_i) - a_i$ and $\bar{d}(p, \mathsf{UE}_{i+1}) \geq d(p, p_{i+1}) - a_{i+1}$. From these observations it follows that

$$d(p, p_i) + d(p, p_{i+1}) - a_i - a_{i+1} \leq \bar{d}(p, \mathsf{UE}_i) + \bar{d}(p, \mathsf{UE}_{i+1}) \leq v_{\max} \cdot (t_{i+1} - t_i),$$

and thus $p \in E^2$. Because $\bar{d}$ always gives a positive value, we also have $d(p, p_i) - a_i \leq \bar{d}(p, \mathsf{UE}_i) \leq v_{\max} \cdot (t_{i+1} - t_i)$, and $p \in D_i$ (and similarly, $p \in D_{i+1}$). This proves the first inclusion.

Next, we show the reverse inclusion $E^2 \cap D_i \cap D_{i+1} \subseteq \mathsf{UPPA}$. Let p be a point in $E \cap D_i \cap D_{i+1}$. We distinguish between three cases. When p lies outside both UE_i and UE_{i+1}, we have $\bar{d}(p, \mathsf{UE}_i) = d(p, p_i) - a_i$ and $\bar{d}(p, \mathsf{UE}_{i+1}) = d(p, p_{i+1}) - a_{i+1}$. Combining this with the assumption that $p \in E^2$ shows that $p \in \mathsf{UPPA}$. Next, we consider the case where p lies in exactly one of UE_i and UE_{i+1}. Let us say (without loss of generality) that $p \in \mathsf{UE}_i$ and $p \notin \mathsf{UE}_{i+1}$. Then $\bar{d}(p, \mathsf{UE}_i) = 0$ and $\bar{d}(p, \mathsf{UE}_{i+1}) = d(p, p_{i+1}) - a_{i+1}$. Now, the assumption that $p \in D_{i+1}$ implies that $p \in \mathsf{UPPA}$. Finally, we are left with the case where p belongs both to UE_i and to UE_{i+1}. In this case however, we trivially have $p \in \mathsf{UPPA}$ because $\bar{d}(p, \mathsf{UE}_i) = \bar{d}(p, \mathsf{UE}_{i+1}) = 0$. This concludes the proof of the second inclusion. □